Customer Directrix Load-Based Demand Response from Prosumer Communities

Zhan Liu, Yue Zhou*, Wei Gan, Fushuan Wen, Hongtao Ren

***Abstract*-- Demand response (DR) based on customer directrix load (CDL) is a new incentive-based DR scheme, typically invited by regional utility grid companies. In this context, a framework is proposed for a prosumer community to participate in CDL-based DR, comprising two key steps: power optimization to balance electricity costs and DR benefits for the overall prosumer community, and cost allocation for prosumers within the community through two hypothetical sub-steps, i.e., cooperation without and with DR. In the power optimization step, the Convex-Concave Procedure (CCP) algorithm is used to relax the non-convex parts of the optimization objective to be linear ones, gradually approximating the optimal solution by iteratively correcting the upper bound function. In the cost allocation step, the Owen value method is applied, which accounts for priority coalitions and eliminates the unrealistic coalition possibilities that are inherent in the calculation of Shapley value. Comprehensive simulations of a test case validate the rationality of the CDL-based DR framework and the effectiveness of the iterative method.**

***Index Terms*—Convex-Concave Procedure (CCP); Customer Directrix Load (CDL); Incentive-Based Demand Response; Owen Value Method; Prosumer Community.**

I. INTRODUCTION

In recent years, with the continuous advancement of global energy transition, distributed energy resources (DERs) have become increasingly prevalent in distribution networks [1]-[4]. These resources, including photovoltaics (PV), electric vehicles (EVs), and energy storages (ESs), etc., enhance the flexibility of power systems [5], [6]. However, they also bring significant changes to various aspects of power systems, posing substantial operational challenges [7]-[9].

Against this backdrop, the concepts of "prosumer" [10] and "prosumer community" [10], [11] have emerged. Prosumers are the owners of DERs who, by installing and operating these resources, not only meet their own energy needs but also feed excess power back into the utility grid. Prosumer communities, composed of multiple prosumers, form interconnected networks that share resources, thereby enhancing overall energy efficiency and economic benefits [12], [13]. These communities involve not only the physical exchange of energy but also information exchange and management mechanisms, aiming primarily at achieving local power and energy consumption and balance [10], [12].

With the rapid growth of DERs and prosumer communities, demand side management (DSM) [14], [15] of power systems has become increasingly crucial. Demand response (DR), as a vital part of DSM, encourages consumers to reduce or shift their electricity usage during certain periods, thereby effectively enhancing the operational efficiency of power systems and improve energy utilization [16]. It is divided into two types: price-based demand response (PDR) and incentive-based demand response (IDR) [17]. For IDR, the response contribution is typically evaluated based on the customer baseline load (CBL) [18]. CBL represents the predicted load curve of consumers if they do not participate in DR. IDR mechanisms designed around CBL have been widely deployed across the world, for applications like peak shaving, valley filling, operating reserves, frequency response, etc.

In recent years, another novel type of IDR has been proposed, named customer directrix load (CDL)-based DR [19]. In CDL-based DR, DR program operators issue response requirement as a CDL in advance for the DR service providers to follow. CDL can serve as a reference to guide adjustable loads in smoothing out fluctuations from non-dispatchable resources within the power system. For example, [20] proposed a method to create locational CDLs in transmission networks for releasing network congestion. CDL can be directly established according to the needs of the power system, eliminating the need to calculate each consumer's CBL, which is usually a difficult task due to various uncertainties and consumers' potential strategic behaviors.

There have been several studies conducted on CDL-based DR. Ref. [21] examines large-scale aggregated communication base stations, leveraging backup ES flexibility to reshape non-adjustable communication loads, enabling the overall load to follow the CDL. In [22], a cluster of variable-frequency air conditioners was modeled, incorporating second-order equivalent thermal parameters and indoor/outdoor temperatures. A day-ahead rolling control method was then used to track the CDL.

Some studies further considered the interaction between utility grid companies and electricity consumers via game theory. Ref. [23] explored the pricing of CDL-based DR between utility grid companies and clusters of water heaters using a leader-follower game model. A genetic algorithm was

This work was supported by National Key Research and Development Program (2022YFB2403100).

Z. Liu is with the College of Electrical Engineering, Zhejiang University, Hangzhou 310027, China (e-mail: liuzhan22238@zju.edu.cn).

Y. Zhou and W. Gan are both with the School of Engineering, Cardiff University, Cardiff CF24 3AA, UK (e-mail: zhouy68@cardiff.ac.uk; GanW4@cardiff.ac.uk).

F. Wen is with the Hainan Institute, Zhejiang University, Sanya 572000, China, and also with the College of Electrical Engineering, Zhejiang University, Hangzhou 310027, China (e-mail: fushuan.wen@gmail.com).

H. Ren is with State Grid Economic and Technological Research Institute Co., Ltd., Beijing 102209, China (e-mail: rht111222@gmail.com).

used to solve the model. Ref. [24] proposed a CDL-DR pricing mechanism based on a cooperative game model between utility grid operators and aggregators managing heat pumps and EVs. The Nash bargaining was used to solve this model. In [25], a leader-follower game model was developed, optimizing the interests of both the upper-level operator and load aggregator through incentive pricing and load adjustments.

Despite these studies exploring various aspects of CDL-based DR, they mainly focus on resource aggregation by aggregators, emphasizing how aggregators enhance market flexibility and commercial gains. However, the role of local prosumer communities, particularly in the context of CDL-based DR, has not been explored.

In this context, this paper focuses on the mechanisms and strategies for prosumer communities to participate in the CDL-based DR. Two key issues warrant in-depth investigation: first, the economic optimization model of a prosumer community considering CDL-based DR incentives; second, the cost allocation model for the prosumers cooperating in the prosumer community.

For the first issue on economic optimization, a well-designed “incentive function” is usually used to assess the quality of CDL-based DR provided by a service provider and calculate the corresponding service revenue, which is then combined with electricity costs to create an overall economic optimization objective. The commonly used incentive function for CDL-based DR is an exponential function [19]-[22] , due to its continuity and smoothness across the entire domain. This function maps the deviation between the normalized power curve of the service provider and the CDL to the interval [0,1], with smaller deviations resulting in higher incentives. However, in optimization problems, this function leads to a non-convex objective, making it unsolvable by commercial solvers.

To overcome the challenges of non-convex optimization, some studies have replaced exponential functions with linear [23], [24] or quadratic functions [25]. While this approach improves the feasibility and efficiency, it introduces new complexities. These alternative functions often fail to naturally map all deviations to a finite range as exponential functions do, necessitating threshold-based segmentation to map extreme deviations to a fixed value (e.g., 0). This requires careful selection of breakpoints, and inappropriate choices can degrade model performance and complicate implementation and tuning.

Despite these alternatives, non-convex objective functions remain an issue. Current methods, such as those in [21], [22], rely on heuristic algorithms to solve non-convex models, with significant limitations. These algorithms are computationally intensive, and may produce unstable results, with different runs potentially yielding different outcomes, which affects solution consistency and reliability.

Therefore, it is crucial to develop effective methods for handling non-convex objectives, improving both solvability and computational efficiency for economic optimization in CDL-based DR.

For the second issue on cost allocation, cooperation is essential in prosumer communities due to the complementary resources and shared interests among the community members, making it a natural choice for minimizing overall costs. Consequently, cooperative game theory emerges as a key approach. Cooperative game theory-based profit allocation methods include the equal allocation method [26], proportional share method[27], and Shapley value method [28]-[30]. However, the first two methods are only suitable for simple scenarios where the profit distribution is even or proportional to power output. In contrast, the Shapley value method can fairly distribute cooperative gains by considering the marginal contributions of each member to the coalition, widely applied in the benefit allocation of prosumer communities. Ref. [28] uses the Shapley value method to distribute allocations among wind power, PV, and load alliances participating in wholesale markets. Ref. [29] accounts for the responsiveness of flexible loads, such as EVs, air conditioning, and ES, using the Shapley value method to allocate the benefits of their participation in DR. Ref. [30] develops a DR model for an energy system with various electricity and gas users. The model shifts adjustable loads and converts gas loads based on price signals, using the Shapley method to allocate costs among the users.

Although the Shapley value method is widely recognized and extensively used, it assumes that all coalitions are equally likely and independent, which does not always reflect the complex cooperative relationships in real-world prosumer communities. It calculates each participant's contribution by averaging their marginal contributions across all possible coalitions, ensuring a fair distribution of cooperative gains. A participant’s marginal contribution is determined by adding it to an existing coalition and measuring the incremental benefit. While mathematically rigorous, the method assumes that all coalitions, regardless of their feasibility or practicality, are equally likely to form. In practice, some prosumers may form internal priority coalitions due to factors like geography, resource characteristics, or existing partnerships, and these coalitions act as single entities when dealing with other prosumers. This means some coalitions considered by the Shapley value method may never actually form, leading to allocations that do not match real-world scenarios. Therefore, another allocation method is needed to ensure all participants fairly benefit from shared energy and power adjustments, promoting cooperation and resource optimization among prosumers.

In summary, by deeper exploring the above two key issues, an innovative framework is proposed in this paper for a prosumer community to participate in CDL-based DR. The main contributions are:

(1) A CDL-based DR mechanism is proposed, including two steps: power optimization to balance electricity costs and DR benefits for the overall prosumer community, and cost allocation for prosumers within the community through two hypothetical sub-steps, i.e., cooperation without and with DR.

(2) The Owen value method, accounting for priority coalitions, is introduced for cost allocation. Unlike the traditional Shapley method, the Owen method evaluates each prosumer's marginal contribution while reflecting actual coalition structures, excluding theoretical coalitions that do not exist in practice.

(3) The convex-concave procedure (CCP) algorithm is used to deal with the non-convex issue. By constructing appropriate upper bound functions of the objective function and optimizing these upper bounds in each iteration, the original problem is decomposed into multiple iterative convex subproblems.

The rest of the paper is organized as follows. Section II outlines the architecture of a prosumer community and the formulation of the two-step framework. Section III presents the mathematical models. Section IV introduces the solution procedure. Section V shows the simulation results and analysis. Finally, Section VI concludes the paper.

II. Problem Formulation

A. Architecture of a prosumer community

As shown in Fig. 1, the types of prosumers include PV operators, residential users (RUs) with flexible loads, parking lot operators with charging stations (CS), and distributed ES operators.

Assume there are $|\boldsymbol{J}|$ prosumers in a distribution network area. The prosumer index is denoted as *j*, where $\boldsymbol{J}=\{1,2,...,|\boldsymbol{J}|\}$, $j\in\boldsymbol{J}$. Prosumers 1-4 in Fig. 1 represent four different types of prosumers, respectively.

Prosumers form a community where they share energy internally. Only when there is an overall deficit or surplus will the community buy/sell electricity from/to the regional utility grid company.

Some prosumers may join the community as a priority coalition. For example, some PV operators may prefer to reach contracts with the prosumers with geographic proximity or specific operational modes to prioritize local energy consumption. Prosumers 1 and 2 in Fig. 1 represent a priority coalition, shown by a black dashed box.

In IDR, the prosumer community acts as a whole, adjusting its power according to the utility grid company's DR instructions. CDL-based DR is a considered in this paper. The CDL is a normalized power signal retaining only shape characteristics. It provides a power-shaping target for all DR participants. The utility grid calculates response performance based on the power curve shapes of the prosumer community and then remunerate the community based on the performance.

B. Formulation of the two-step operation strategy

As shown in Fig. 1, the operation framework of the prosumer community consists of two steps.

1) Step 1: Total cost minimization

The total operation cost C^{Com} of the prosumer community is given by:

$$C^{\mathrm{Com}}=-R^{\mathrm{CDL}}+C^{\mathrm{E}} \tag{1}$$

where R^{CDL} is the revenue from CDL-based DR, and C^{E} is the cost of electricity from the utility grid.

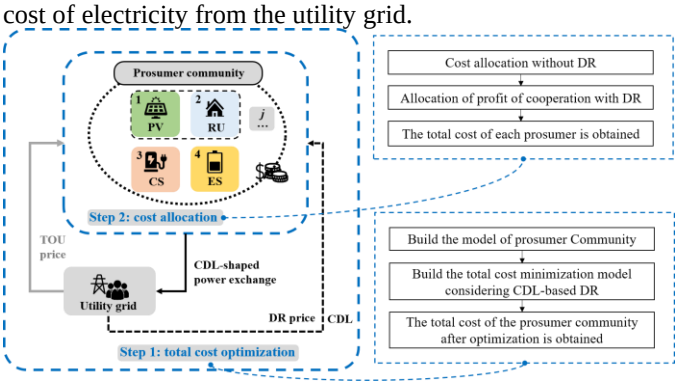

Fig. 1 Overview of the proposed architecture of the prosumer community.

When participating in CDL-based DR, the prosumer community needs to adjust its overall power curve to match the CDL as closely as possible to earn incentive revenue. Meanwhile, the community needs to balance the cost of electricity and the revenue from DR to minimize the total cost.

2) Step 2: Cost allocation

After the prosumer community finishes the total cost optimization, the total cost needs to be distributed among the prosumers in the community.

The cost allocation consists of two hypothetical sub-steps. In the first sub-step, prosumers form a community, achieving local consumption and reducing electricity costs. In the second sub-step, the community participates in CDL-based DR, earning incentive compensation by sacrificing some electricity costs. Sub-step 1 allocates the total cost without cooperation, while sub-step 2 allocates the net profits from DR.

In sub-step 2, the allocation requires calculating the marginal contributions of each prosumer. The commonly used Shapley value method calculates these based on the total cost of all possible subsets of prosumers. However, as noted earlier, some subsets do not exist. Therefore, the proposed method needs to consider actual possible coalitions and exclude non-existent subsets from the coalition set.

The above provides an overview of the operation framework for the prosumer community. R^{CDL} and C^{E} will be modeled in the next section, followed by the total cost minimization model (Step 1) and the cost allocation model (Step 2).

III. Mathematical Modeling

A. Model of CDL-based DR

Let a day be divided into *T* periods. The CDL curve issued by the regional utility grid company is denoted as $\boldsymbol{P}^{\mathrm{CDL},*}$ for $t\in[1,T]$, where $P_t^{\mathrm{CDL},*}=\left[\boldsymbol{P}^{\mathrm{CDL},*}\right]_t$ represents the CDL at time period *t*. The given CDL value is a normalized power value, satisfying $\sum_{t=1}^{T}P_t^{\mathrm{CDL},*}=1$. It retains only the shape characteristics.

The incentive compensation for the service provider can be calculated in three steps.

Firstly, the service provider calculates the normalized power value $P_t^{\mathrm{Com},*}$ at time *t* using equation (2), forming a normalized power curve $\boldsymbol{P}^{\mathrm{Com},*}$ when arranged in time sequence.

$$P_t^{\mathrm{Com},*}=\frac{P_t^{\mathrm{Com}}}{\sum_{t=1}^{T}P_t^{\mathrm{Com}}}=\frac{P_t^{\mathrm{Com}}}{P^{\mathrm{Com}}} \tag{2}$$

where P_t^{Com} is the power value of the service provider at time *t*, P^{Com} is the total power of the service provider declaring ahead day.

Secondly, the similarity index S^{Com} for assessing the DR performance is defined. The Manhattan distance is used to measure the difference between the normalized power vector and the CDL vector. In equation (3), it is first calculated by summing the absolute differences between these two vectors over the entire time period, and then averaged to obtain z^{Com}.

This metric z^{Com} reflects the aggregated deviation across all time periods, considering the difference between the

normalized power values and the CDL at each interval. It plays a crucial role in quantifying the overall DR performance.

Then the similarity S^{Com} can be calculated. Conventionally, an exponential function can be used, as shown in equation (4), but it will be replaced by another originally proposed expression later in this paper.

$$z^{\mathrm{Com}} = \sum_{t=1}^{T} \frac{1}{T} \left| P_t^{\mathrm{Com},*} - P_t^{\mathrm{CDL},*} \right| \tag{3}$$

$$S^{\mathrm{Com}} = \mathrm{e}^{-\frac{1}{\gamma} z^{\mathrm{Com}}} \tag{4}$$

This transformation (4) maps the aggregated deviation into a similarity index within the range [0,1], where smaller deviations lead to higher scores. As discussed in the introduction, the use of exponential functions in CDL-based DR ensures smoothness and continuity, making it suitable for both performance assessment and optimization tasks.

Together, equations (3) and (4) systematically connect the performance evaluation of the service provider with incentive calculations. By quantifying deviations and translating them into similarity scores, these equations establish a reliable framework for assessing DR performance and determining economic rewards in CDL-based DR programs.

Finally, the DR revenue R^{CDL} is calculated as shown in equation (5):

$$R^{\mathrm{CDL}} = \pi^{\mathrm{CDL}} P^{\mathrm{Com}} S^{\mathrm{Com}} \tag{5}$$

where π^{CDL} is the unit incentive compensation paid by the utility grid company to the service provider.

In equation (4), γ is the deviation factor set by the utility grid company. It influences the similarity index S^{Com} and subsequently the calculation of DR revenue in equation (5). Adjusting γ allows the utility grid to modulate the sensitivity of S^{Com} to deviations. A higher γ value tends to lessen the impact of deviations, leading to a milder change in similarity. Conversely, a lower γ value makes S^{Com} more sensitive to deviations, resulting in a more noticeable effect on similarity and DR revenue. This enables the utility grid to fine-tune the incentives to achieve the desired outcomes in CDL-based DR.

B. Model of the prosumer community

Let $\boldsymbol{Id} = \{\mathrm{PV},\mathrm{CP},\mathrm{CS},\mathrm{ES}\}$, $\mathrm{Id} \in \boldsymbol{Id}$, where Id represents the types of prosumers. The sets of indices for these prosumers are denoted as $\boldsymbol{J}_{\mathrm{PV}}$, $\boldsymbol{J}_{\mathrm{CP}}$, $\boldsymbol{J}_{\mathrm{CS}}$, $\boldsymbol{J}_{\mathrm{ES}}$, respectively. These sets satisfy:

$$\begin{cases} \bigcap\limits_{\mathrm{Id} \neq \mathrm{Id}'} \left(\boldsymbol{J}_{\mathrm{Id}} \cap \boldsymbol{J}_{\mathrm{Id}'} \right) = \varnothing \\ \bigcup\limits_{\mathrm{Id} \in \boldsymbol{Id}} \boldsymbol{J}_{\mathrm{Id}} = \boldsymbol{J} \end{cases} \tag{6}$$

The model of the prosumer community is given in equations (7) - (13):

$$C^{\mathrm{E}} = \sum_{t=1}^{T} \left(\pi_t^{\mathrm{TOU}} P_t^{\mathrm{buy}} + \pi_t^{\mathrm{FIT}} P_t^{\mathrm{sell}} \right) \cdot \Delta T \tag{7}$$

$$\pi_t^{\mathrm{TOU}} > \pi_t^{\mathrm{FIT}} \tag{8}$$

$$P_t^{\mathrm{buy}} + P_t^{\mathrm{sell}} = P_t^{\mathrm{Com}} \tag{9}$$

$$P_t^{\mathrm{buy}} \cdot P_t^{\mathrm{sell}} = 0 \tag{10}$$

$$0 \le P_t^{\mathrm{buy,min}} \le P_t^{\mathrm{buy}} \le P_t^{\mathrm{buy,max}} \tag{11}$$

$$P_t^{\mathrm{sell,min}} \le P_t^{\mathrm{sell}} \le P_t^{\mathrm{sell,max}} \le 0 \tag{12}$$

$$P_t^{\mathrm{Com}} = \begin{bmatrix} \sum\limits_{j \in J_{\mathrm{PV}}} P_{j,t}^{\mathrm{PV}} \\ + \sum\limits_{j \in J_{\mathrm{CP}}} P_{j,t}^{\mathrm{Load}} \\ + \sum\limits_{j \in J_{\mathrm{CS}}} \left(P_{j,t}^{\mathrm{CS,ch}} - P_{j,t}^{\mathrm{CS,dis}} \right) \\ + \sum\limits_{j \in J_{\mathrm{ES}}} \left(P_{j,t}^{\mathrm{ES,ch}} - P_{j,t}^{\mathrm{ES,dis}} \right) \end{bmatrix} \tag{13}$$

where π_t^{TOU} and π_t^{FIT} are the time-of-use (TOU) price and feed-in tariff (FIT) of the utility grid at time *t*, respectively. P_t^{buy} and P_t^{sell} are the total power bought and sold by the prosumer community with the utility grid at time *t*. $P_t^{\mathrm{buy,min}}$ and $P_t^{\mathrm{buy,max}}$ are the minimum and maximum power that the prosumer community can buy from the utility grid at time *t*, respectively. $P_t^{\mathrm{sell,min}}$ and $P_t^{\mathrm{sell,max}}$ are the minimum and maximum power that the prosumer community can sell to the utility grid at time *t*, respectively. $P_{j,t}^{\mathrm{PV}}$, $P_{j,t}^{\mathrm{Load}}$, $P_{j,t}^{\mathrm{CS,ch}}$, $P_{j,t}^{\mathrm{CS,dis}}$, $P_{j,t}^{\mathrm{ES,ch}}$ and $P_{j,t}^{\mathrm{ES,dis}}$ are the PV feed-in power, residential load power, CS charging power, CS discharging power, ES charging power, and ES discharging power of prosumer *j* at time *t*, respectively.

Equation (7) represents the total electricity cost of the prosumer community. Equation (8) indicates that π_t^{TOU} must be greater than π_t^{FIT}. Equation (9) defines P_t^{buy} and P_t^{sell} as the positive and negative components of the community's total power P_t^{Com} at each time and equation (10) avoids the prosumer community to buy and sell electricity at the same time. In this optimization problem, due to the constraint in Equation (8), P_t^{buy} and P_t^{sell} are unlikely to both be zero simultaneously, allowing Equation (10) to be omitted [31]. Equations (11) and (12) establish the boundary constraints for P_t^{buy} and P_t^{sell}. Equations (13) represents P_t^{Com} as the sum of power from different types of prosumers at time period *t*: PV, RU, CS and ES.

After establishing the model of the prosumer community, individual constraints for each type of prosumer need to be considered as well, detailed as below.

1) Distributed PV operators. These operators install small solar PV systems on rooftops, the ground, or other suitable locations to supply electricity to the regional grid. The PV feed-in power is constrained by:

$$0 \le P_{j,t}^{\mathrm{PV}} \le P_{j,t}^{\mathrm{PV,max}} \tag{14}$$

where $P_{j,t}^{\mathrm{PV,max}}$ are the maximum value of PV feed-in power of prosumer *j* at time *t*.

2) RUs with flexible loads. In residential households, fixed loads $P_{j,t}^{\mathrm{Load,f}}$ are not affected by electricity prices. Transferable flexible loads $P_{j,t}^{\mathrm{Load,move}}$ are sensitive to prices and can be shifted across different time periods. The model is given by:

$$\sum_{t=1}^{T} P_{j,t}^{\mathrm{Load,move}} \Delta t = 0 \tag{15}$$

$$P_{j,t,\min}^{\mathrm{Load,move}} \le P_{j,t}^{\mathrm{Load,move}} \le P_{j,t,\max}^{\mathrm{Load,move}} \tag{16}$$

$$P_{j,t}^{\mathrm{Load}} = P_{j,t}^{\mathrm{Load,f}} + P_{j,t}^{\mathrm{Load,move}} \tag{17}$$

where $P_{j,t,\min}^{\text{Load,move}}$ and $P_{j,t,\max}^{\text{Load,move}}$ are the minimum and maximum flexible loads at time *t*. Equation (15) represents the balance constraint for transferable flexible loads, ensuring that the total flexible load remains unchanged within an adjustment cycle. Equation (16) specifies the upper and lower adjustment limits for transferable flexible loads. Equation (17) clarifies that total flexible loads consist of both transferable and fixed parts.

3) Parking lot operators with CS. They provide charging facilities in parking lots to meet the needs of EV charging. They offer parking and charging services and aggregate EV resources.

The arrival and departure information of EVs for the day-ahead schedule is known. The overall modeling of the CS uses the outer approximation of the Minkowski sum method[32].

The CS decision variables are $P_{j,t}^{\text{CS,ch}}$, $P_{j,t}^{\text{CS,dis}}$ and $E_{j,t}^{\text{CS}}$, representing the total charging power, total discharging power, and total battery energy at time *t*. The EV decision variables are $P_{j,n,t}^{\text{EV,ch}}$, $P_{j,n,t}^{\text{EV,dis}}$ and $E_{j,n,t}^{\text{EV}}$, representing the charging power, discharging power, and battery energy of EV *n* connected to prosumer *j*'s CS at time *t*. These decision variables satisfy the following constraints:

$$P_{j,t}^{\text{CS,ch}} = \sum_{n=1}^{N} P_{j,n,t}^{\text{EV,ch}} \tag{18}$$

$$P_{j,t}^{\text{CS,dis}} = \sum_{n=1}^{N} P_{j,n,t}^{\text{EV,dis}} \tag{19}$$

$$E_{j,t}^{\text{CS}} = \sum_{n=1}^{N} E_{j,n,t}^{\text{EV}} \tag{20}$$

Set the CS parameters $P_{j,t}^{\text{CS,ch,max}}$, $P_{j,t}^{\text{CS,dis,max}}$, $E_{j,t}^{\text{CS,min}}$, $E_{j,t}^{\text{CS,max}}$ and $\Delta E_{j,t}^{\text{CS}}$. These represent the maximum total charging power, maximum total discharging power, minimum total battery energy, maximum total battery energy, and the energy change due to EV connection status at time *t* for prosumer *j*. Set the EV parameters $P_{j,n}^{\text{EV,ch,max}}$, $P_{j,n}^{\text{EV,dis,max}}$, $E_{j,n}^{\text{EV,min}}$, $E_{j,n}^{\text{EV,max}}$, $E_{j,n,\text{arr}}^{\text{EV}}$, $E_{j,n,\text{dep}}^{\text{EV}}$ and $\nu_{j,n,t}^{\text{EV}}$, where $\nu_{j,n,t}^{\text{EV}} = \{0,1\}$. These represent the maximum charging power, maximum discharging power, minimum battery energy, maximum battery energy, battery energy upon arrival, battery energy upon departure, and connection status of EV *n* at time *t* for prosumer *j*. These parameters satisfy the following constraints:

$$P_{j,t}^{\text{CS,ch,max}} = \sum_{n=1}^{N} \nu_{j,n,t}^{\text{EV}} P_{j,n}^{\text{EV,ch,max}} \tag{21}$$

$$P_{j,t}^{\text{CS,dis,max}} = \sum_{n=1}^{N} \nu_{j,n,t}^{\text{EV}} P_{j,n}^{\text{EV,dis,max}} \tag{22}$$

$$E_{j,t}^{\text{CS,min}} = \sum_{n=1}^{N} \nu_{j,n,t}^{\text{EV}} E_{j,n}^{\text{EV,min}} \tag{23}$$

$$E_{j,t}^{\text{CS,max}} = \sum_{n=1}^{N} \nu_{j,n,t}^{\text{EV}} E_{j,n}^{\text{EV,max}} \tag{24}$$

$$\Delta E_{j,t}^{\text{CS}} = \sum_{n=1}^{N} \begin{bmatrix} E_{j,n,\text{arr}}^{\text{EV}} \nu_{j,n,t}^{\text{EV}} \left(\nu_{j,n,t}^{\text{EV}} - \nu_{j,n,t-1}^{\text{EV}} \right) \\ -E_{j,n,\text{dep}}^{\text{EV}} \nu_{j,n,t-1}^{\text{EV}} \left(\nu_{j,n,t-1}^{\text{EV}} - \nu_{j,n,t}^{\text{EV}} \right) \end{bmatrix} \tag{25}$$

The EV-related charging and discharging model (e.g., the constraint ensuring EV users' charging demands are satisfied before departure), as well as the Minkowski sum derivation process, are shown in the Appendix A. The final Minkowski sum formula is:

$$0 \le P_{j,t}^{\text{CS,ch}} \le P_{j,t}^{\text{CS,ch,max}} \tag{26}$$

$$0 \le P_{j,t}^{\text{CS,dis}} \le P_{j,t}^{\text{CS,dis,max}} \tag{27}$$

$$E_{j,t}^{\text{CS,min}} \le E_{j,t}^{\text{CS}} \le E_{j,t}^{\text{CS,max}} \tag{28}$$

$$E_{j,t}^{\text{CS}} = E_{j,t-1}^{\text{CS}} + \Delta E_{j,t}^{\text{CS}} + \left(\eta_{\text{EV,ch}} P_{j,t}^{\text{CS,ch}} - \frac{1}{\eta_{\text{EV,dis}}} P_{j,t}^{\text{CS,dis}} \right) \Delta t \tag{29}$$

where $\eta_{\text{EV,ch}}$ and $\eta_{\text{EV,dis}}$ are the charging and discharging efficiencies of the EVs, respectively.

4) Distributed ES ***operators.*** Distributed ES systems are devices deployed near power users or other distributed resources to store and release electrical energy. The model is given by:

$$0 \le P_{j,t}^{\text{ES,ch}} \le P_{j}^{\text{ES,ch,max}} \tag{30}$$

$$0 \le P_{j,t}^{\text{ES,dis}} \le P_{j}^{\text{ES,dis,max}} \tag{31}$$

$$P_{j,t}^{\text{ES,ch}} \cdot P_{j,t}^{\text{ES,dis}} = 0 \tag{32}$$

$$E_{j,\min}^{\text{ES}} \le E_{j,t}^{\text{ES}} \le E_{j,\max}^{\text{ES}} \tag{33}$$

$$E_{j,t}^{\text{ES}} = E_{j,t-1}^{\text{ES}} + \left(\eta_{\text{ES,ch}} P_{j,t}^{\text{ES,ch}} - \frac{1}{\eta_{\text{ES,dis}}} P_{j,t}^{\text{ES,dis}} \right) \Delta t \tag{34}$$

$$E_{j,T}^{\text{ES}} = E_{j,0}^{\text{ES}} \tag{35}$$

where $P_{j,t}^{\text{ES,ch}}$ and $P_{j,t}^{\text{ES,dis}}$ are the charging and discharging power at time *t*, $P_{j}^{\text{ES,ch,max}}$ and $P_{j}^{\text{ES,dis,max}}$ are the maximum charging and discharging power at time t. $E_{j,t}^{\text{ES}}$ is the stored energy, $E_{j,\min}^{\text{ES}}$ and $E_{j,\max}^{\text{ES}}$ are the minimum and maximum stored energy. $E_{j,0}^{\text{ES}}$ and $E_{j,T}^{\text{ES}}$ are the initial and final stored energy, respectively. $\eta_{\text{ES,ch}}$ and $\eta_{\text{ES,dis}}$ are the charging and discharging efficiencies.

Ref. [31] proves that with efficiencies less than 100%, storage will not charge and discharge simultaneously, so constraint (32) is ignored.

C. Model of total cost minimization as the first step of the operation framework

In summary, the prosumer community aims to minimize the overall cost while participating in CDL-based DR initiated by the utility grid company. The following optimization model is obtained:

$$\min C^{\text{Com}} = \left\{ \begin{array}{l} -\pi^{\text{CDL}} P^{\text{DL}} \mathrm{e}^{-\frac{1}{\gamma} z^{\text{DL}}} \\ +\sum_{t=1}^{T} \left(\pi_t^{\text{buy}} P_t^{\text{buy}} + \pi_t^{\text{sell}} P_t^{\text{sell}} \right) \Delta t \end{array} \right\} \tag{36}$$

s.t. (2)-(3), (11), (12), (13), (14)-(17), (26)-(35).

This optimization model corresponds to step 1 in Fig. 1. Due to the non-convex nature of this model, further analysis of its handling will be conducted in Section IV.

D. Model of cost allocation using Owen Value Method as the second step of the operation framework

This model of cost allocation corresponds to step 2 in Fig. 1. Fig. 2 illustrates the cost allocation for the prosumer community, divided into two assumed sub-steps for calculation and analysis. The vertical axis lists cost types, while the horizontal axis shows cost values qualitatively.

Mathematically, the total cost reduction arises from the balance between DR incentives and additional electricity costs incurred during DR. The total cost with DR $C^{\text{Com},(2)}$ is calculated by equation (1). It is the cost to be allocated and is divided into two parts: total cost without DR $C^{\text{Com},(1)}$ and net profits from DR

$\left(C^{\mathrm{Com},(1)}-C^{\mathrm{Com},(2)}\right)$ .Sub-step 1 allocates the total cost without cooperation, while sub-step 2 allocates the net profits from DR. In the second sub-step, the community engages in CDL-based DR, earning incentive compensation while incurring relatively small additional electricity costs. This results in net profits, reducing the total cost from $C^{\mathrm{Com},(1)}$ to $C^{\mathrm{Com},(2)}$, despite the additional increase in electricity costs from $C^{\mathrm{E},(1)}$ to $C^{\mathrm{E},(2)}$.

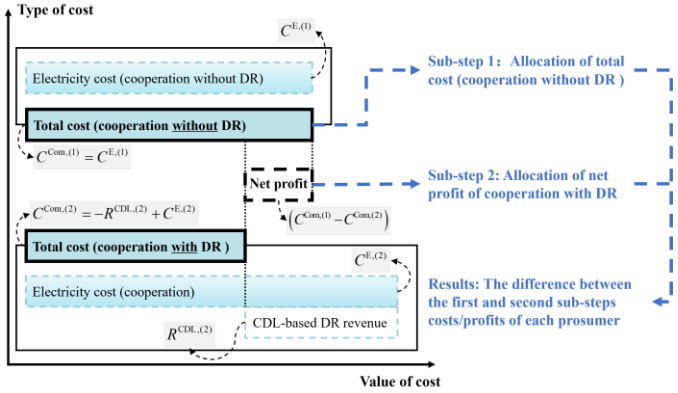

Fig. 2 Overview of the two sub-steps in cost allocation step.

Fig. 2 provides the illustration, with the length of rectangles along the horizontal axis representing the magnitudes of cost components. The length of the "electricity cost (cooperation without DR)" rectangle equals to that of the "total cost (cooperation without DR)" rectangle, forming the baseline cost. With DR implemented, the longer "electricity cost (cooperation with DR)" rectangle reflects increased electricity expenses, while the shorter "total cost (cooperation with DR)" rectangle shows the overall reduced cost after accounting for DR incentives. The net cost reduction is visually depicted by the difference in lengths between the "total cost (cooperation without DR)" and "total cost (cooperation with DR)" rectangles.

1) First sub-step: Prosumers form a community through cooperation, sharing energy locally to lower electricity costs by reducing dependence on the utility grid. Participation in CDL-based DR is not considered at this stage.

During energy sharing, some prosumers may trade preferentially with specific others, forming priority coalitions. Each such priority coalition then trades as a whole with other independent prosumers. The Shapley value method considers all $2^{|J|}$ possible coalitions (including the empty set), assuming equal likelihood for each coalition to form. While mathematically rigorous, this approach often includes unrealistic coalitions that are unlikely to form in practice. To ensure fair cost allocation, the Owen value method is used[33]. This method extends the Shapley value method by considering contributions within and between priority coalitions, reflecting real-world scenarios by including only possible coalitions and excluding non-existent ones. Furthermore, the Owen value method allocates costs based on prosumers' marginal contributions, ensuring incentive compatibility in cost allocation. This approach ensures fair benefits for all participants in energy sharing and power adjustment. The Owen value method formula is as follows, aligning individual incentives with the collective goals of the prosumer community.

Let $\boldsymbol{J}$ be the set of prosumer indices. Suppose the prosumers are divided into *m* disjoint priority coalitions, then $\boldsymbol{J}=\{\boldsymbol{J}_1,\boldsymbol{J}_2,\ldots,\boldsymbol{J}_k,\ldots,\boldsymbol{J}_m\}$, $\boldsymbol{J}_k\subseteq\boldsymbol{J}$, where $\boldsymbol{J}_k$ refers to the *k*th priority coalition.

Allocation of costs among priority coalitions: Each priority coalition is treated as a single entity trading with others, and the Shapley value formula is used to calculate the cost (the negative value means benefit) distribution ψ_{J_k} among the priority coalitions:

$$\psi_{J_k}=\sum_{\boldsymbol{H}\subseteq\boldsymbol{J}}\frac{(|\boldsymbol{H}|-1)!(|\boldsymbol{J}|-|\boldsymbol{H}|)!}{|\boldsymbol{J}|!}\left(v(\boldsymbol{H})-v(\boldsymbol{H}-\{\boldsymbol{J}_k\})\right) \tag{37}$$

where $\boldsymbol{H}$ is a coalition containing priority coalition $\boldsymbol{J}_k$. $|\boldsymbol{H}|$ represents the number of priority coalitions and individual prosumers in coalition $\boldsymbol{H}$. $|\boldsymbol{J}|$ represents the number of prosumers in set $\boldsymbol{J}$. $v(\boldsymbol{H})$ represents the total cost of coalition $\boldsymbol{H}$.

Allocation of cost within priority coalitions: The calculated cost ψ_{J_k} for each priority coalition replaces the value of $v(\boldsymbol{J}_k)$. Within each priority coalition $\boldsymbol{J}_k$, the Shapley value formula is used to allocate the Owen value $\psi_j^{J_k}$ among participants, resulting in the final cost allocation $C_j^{(1)}$ for prosumer *j*.

$$v(\boldsymbol{J}_k)=\psi_{J_k} \tag{38}$$

$$\psi_j^{J_k}=\sum_{\boldsymbol{S}\subseteq\boldsymbol{J}_k}\frac{(|\boldsymbol{S}|-1)!(|\boldsymbol{J}_k|-|\boldsymbol{S}|)!}{|\boldsymbol{J}_k|!}\left(v(\boldsymbol{S})-v(\boldsymbol{S}-\{j\})\right) \tag{39}$$

$$C_j^{(1)}=\psi_j^{J_k} \tag{40}$$

where $\boldsymbol{S}$ is any coalition within $\boldsymbol{J}_k$ that includes prosumer *j*. $|\boldsymbol{S}|$ represents the number of prosumers in coalition $\boldsymbol{S}$. $|\boldsymbol{J}_k|$ represents the number of prosumers in priority coalition $\boldsymbol{J}_k$. $v(\boldsymbol{S})$ represents the cost (when positive) / benefit (negative) of coalition $\boldsymbol{S}$.

***2) Second Sub-Step*:** In this sub-step, the prosumer community is considered to participate in the CDL-based DR.

While individual prosumers may have DR potential, only the entire prosumer community's participation is considered to maximize the overall benefits and ensure stability to prioritize local consumption. Prosumers may incur more electricity costs but will receive greater CDL-based DR revenue, thus having a lower total cost than that in the first sub-step one, as shown in Fig. 2. Since the DR is designed for the whole community, the marginal costs of individual prosumers are indistinguishable. Therefore, net profits of DR are allocated based on each prosumer's power adjustment compared to that in the first sub-step, i.e., using the first sub-step results as a baseline.

Net profit allocation result of cooperation with DR: As shown in equation (41), prosumer *j*'s contribution is defined as the proportion $I_j^{(2)}$ of their power adjustment to the total power adjustments of all prosumers. Equation (42) multiplies this contribution by the community's net profit with DR to determine prosumer *j*'s contribution, allocating $R_j^{(2)}$ to the prosumer *j*.

$$I_j^{(2)} = \frac{\sum_{t=1}^{T}\left|P_{j,t}^{\mathrm{Id},(2)} - P_{j,t}^{\mathrm{Id},(1)}\right|}{\sum_{j\in J}\sum_{t=1}^{T}\left|P_{j,t}^{\mathrm{Id},(2)} - P_{j,t}^{\mathrm{Id},(1)}\right|} \tag{41}$$

$$R_j^{(2)} = I_j^{(2)}\left(C^{\mathrm{Com},(1)} - C^{\mathrm{Com},(2)}\right) \tag{42}$$

The difference between the first and second sub-step costs/net profits gives the total cost C_j for each prosumer *j* in equation (43).

$$C_j = C_j^{(1)} - R_j^{(2)} \tag{43}$$

IV. Reformulation for Solving the Operation Framework

This section focuses on addressing the non-convex parts of the model of step 1 of the framework. Firstly, the absolute value equation (3) is relaxed to inequality constraints. Secondly, for the non-convex term $\mathrm{e}^{-\frac{1}{\gamma}\sum_{t=1}^{T}\frac{1}{T}\left|P_t^{\mathrm{Com},*} - P_t^{\mathrm{CDL},*}\right|}$ in the objective function (36), the CCP method is used to construct the upper bound function. This approach transforms the non-convex problem into multiple iterative convex subproblems[34]. Finally, a schematic diagram of the improved two-step framework is presented.

A. Relaxation method of absolute value in step 1

Combining equations (2) and (3), let:

$$x_t = \frac{P_t^{\mathrm{Com}}}{P^{\mathrm{Com}}} - P_t^{\mathrm{CDL},*} \tag{44}$$

Combining equations (13) and (44), x_t is defined as:

$$x_t = \frac{1}{P^{\mathrm{Com}}}\begin{bmatrix}\sum_{j\in J_{\mathrm{PV}}} P_{j,t}^{\mathrm{PV}} \\ +\sum_{j\in J_{\mathrm{CP}}} P_{j,t}^{\mathrm{Load}} \\ +\sum_{j\in J_{\mathrm{CS}}}\left(P_{j,t}^{\mathrm{CS,ch}} - P_{j,t}^{\mathrm{CS,dis}}\right) \\ +\sum_{j\in J_{\mathrm{ES}}}\left(P_{j,t}^{\mathrm{ES,ch}} - P_{j,t}^{\mathrm{ES,dis}}\right)\end{bmatrix} - P_t^{\mathrm{CDL},*} \tag{45}$$

The auxiliary decision variable z_t is defined as：

$$z_t = \left|x_t\right| \tag{46}$$

This can be relaxed into a linear inequality constraint:

$$\begin{cases} z_t \geq x_t \\ z_t \geq -x_t \end{cases} \tag{47}$$

Substituting equation (46) into equation (3) gives:

$$z^{\mathrm{Com}} = \sum_{t=1}^{T}\frac{1}{T} z_t \tag{48}$$

In fact, the equality constraint in equation (46) is equivalent to the following linear inequality constraints (49), composed of the infimum constraints (a) and (b) and the supremum constraints (c) and (d). M is a large positive constant.

$$\begin{cases} z_t \geq x_t & (a) \\ z_t \geq -x_t & (b) \\ z_t \leq x_t + (1-u_t)M & (c) \\ z_t \leq -x_t + u_t M & (d) \end{cases}, u_t \in \{0,1\} \tag{49}$$

In the objective function in equation (36), $\mathrm{e}^{-\frac{1}{\gamma}\sum_{t=1}^{T}\frac{1}{T}\left|x_t\right|}$ is monotonically increasing with respect to $\left|x_t\right|$. During minimization, the goal is to keep $\left|x_t\right|$ as small as possible. Constraints (a) and (b) in equation (49) ensure $z_t \geq \left|x_t\right|$, and then the optimization algorithm will naturally choose $z_t = \left|x_t\right|$. Therefore, the supremum constraints (c) and (d) in equation (49) are redundant. The equality constraint in equation (46) can be relaxed to the inequality constraint in equation (47) , including only the infimum inequality constraints (a) and (b) from (49).

B. Convex-concave procedure (CCP) method used in step 1

Let:

$$\boldsymbol{\theta} = [z^{\mathrm{Com}}, P_t^{\mathrm{buy}}, P_t^{\mathrm{sell}}]^{\mathrm{T}} \tag{50}$$

Then:

$$C^{\mathrm{E}}(\boldsymbol{\theta}) = C^{\mathrm{E}}\left(P_t^{\mathrm{buy}}, P_t^{\mathrm{sell}}\right) = \sum_{t=1}^{T}\left(\pi_t^{\mathrm{TOU}} P_t^{\mathrm{buy}} + \pi_t^{\mathrm{FIT}} P_t^{\mathrm{sell}}\right)\Delta t \tag{51}$$

$$R^{\mathrm{CDL}}(\boldsymbol{\theta}) = R^{\mathrm{CDL}}\left(z^{\mathrm{Com}}\right) = \pi^{\mathrm{CDL}} P^{\mathrm{Com}} \mathrm{e}^{-\frac{1}{\gamma} z^{\mathrm{Com}}} \tag{52}$$

$$C^{\mathrm{Com}}(\boldsymbol{\theta}) = -R^{\mathrm{CDL}}(\boldsymbol{\theta}) + C^{\mathrm{E}}(\boldsymbol{\theta}) \tag{53}$$

Both $R^{\mathrm{CDL}}(\boldsymbol{\theta})$ and $C^{\mathrm{E}}(\boldsymbol{\theta})$ are convex functions, with the proof referring to [35] (the definitions of “convex” and “concave” also follow the conventions outlined in [35]). By contrast, the objective function $C^{\mathrm{Com}}(\boldsymbol{\theta})$, being a convex $C^{\mathrm{E}}(\boldsymbol{\theta})$ minus another convex function $R^{\mathrm{CDL}}(\boldsymbol{\theta})$, forms a "convex minus convex" structure. This structure is generally non-convex, according to the verification method described in [35], by analyzing the Hessian matrix of $C^{\mathrm{Com}}(\boldsymbol{\theta})$. Consequently, the optimization problem with $\min C^{\mathrm{Com}}(\boldsymbol{\theta})$ as the objective function is a non-convex one, which cannot be solved using commercial solvers.

For non-convex objective functions, the Majorization-Minimization (MM) algorithm is often used for approximation. Given that $C^{\mathrm{Com}}(\boldsymbol{\theta})$ can be decomposed into a convex function $C^{\mathrm{E}}(\boldsymbol{\theta})$ and a concave function $-R^{\mathrm{CDL}}(\boldsymbol{\theta})$, the non-convex part $-R^{\mathrm{CDL}}(\boldsymbol{\theta})$ can be linearized via a first-order Taylor expansion. This method, known as the Convex-Concave Procedure algorithm [34], is a specific case of the MM algorithm. This linearization simplifies the optimization problem by replacing the non-convex objective with a convex approximation, aligning with MM’s core idea of constructing iteration objective functions. Further insights into the relationship between CCP and MM can be found in [36].

In this study, the CCP algorithm is applied to solve the problem. Choose an initial point $\left(\boldsymbol{\theta}_0, R^{\mathrm{CDL}}\left(\boldsymbol{\theta}_0\right)\right)$ as the first-order Taylor expansion point, construct the upper bound function $\hat{R}^{\mathrm{CDL}}\left(\boldsymbol{\theta}_0\right)$, and obtain the CCP objective function $\hat{C}^{\mathrm{Com}}\left(\boldsymbol{\theta};\boldsymbol{\theta}_0\right) = -\hat{R}^{\mathrm{CDL}}\left(\boldsymbol{\theta};\boldsymbol{\theta}_0\right) + C^{\mathrm{E}}(\boldsymbol{\theta})$. Solve the convex optimization subproblem $\min \hat{C}^{\mathrm{Com}}\left(\boldsymbol{\theta};\boldsymbol{\theta}_0\right)$ to obtain the solution $\boldsymbol{\theta}_1$. Then, compute the original objective function value $C^{\mathrm{Com}}\left(\boldsymbol{\theta}_1\right)$. If $C^{\mathrm{Com}}\left(\boldsymbol{\theta}_0\right) - C^{\mathrm{Com}}\left(\boldsymbol{\theta}_1\right) > \varepsilon$, convergence has not been achieved, and the iteration should proceed.

In the k+1 iteration, the first-order Taylor expansion of the

function $R^{\mathrm{CDL}}(\boldsymbol{\theta})$ at $\left(\boldsymbol{\theta}_k, R^{\mathrm{CDL}}(\boldsymbol{\theta}_k)\right)$ is:

$$\begin{aligned}&\hat{R}^{\mathrm{CDL}}\left(\boldsymbol{\theta};\boldsymbol{\theta}_k\right)=\hat{R}^{\mathrm{CDL}}\left(z^{\mathrm{Com}};z^{\mathrm{Com}_i(k)}\right)\\&=R^{\mathrm{CDL}}\left(z^{\mathrm{Com}_i(k)}\right)+\nabla R^{\mathrm{CDL}}\left(z^{\mathrm{Com}_i(k)}\right)^{\mathrm{T}}\left(z^{\mathrm{Com}}-z^{\mathrm{Com}_i(k)}\right)\\&=\left\{\begin{array}{l}\pi^{\mathrm{CDL}}P^{\mathrm{Com}}\mathrm{e}^{-\frac{1}{\gamma}z^{\mathrm{Com}_i(k)}}\\-\dfrac{1}{\gamma}\pi_t^{\mathrm{CDL}}P^{\mathrm{Com}}\mathrm{e}^{-\frac{1}{\gamma}z^{\mathrm{Com}_i(k)}}\left(z^{\mathrm{Com}}-z^{\mathrm{Com}_i(k)}\right)\end{array}\right\}\end{aligned}\tag{54}$$

Thus, in the k+1 iteration:

$$\hat{C}^{\mathrm{Com}}\left(\boldsymbol{\theta};\boldsymbol{\theta}_k\right)=-\hat{R}^{\mathrm{CDL}}\left(\boldsymbol{\theta};\boldsymbol{\theta}_k\right)+C^{\mathrm{E}}\left(\boldsymbol{\theta}\right)\tag{55}$$

The k+1 sub-problem becomes:

$$\min_{z_t,x_t}\hat{C}^{\mathrm{Com}}=\left\{\begin{array}{l}-\pi^{\mathrm{CDL}}P^{\mathrm{Com}}\mathrm{e}^{-\frac{1}{\gamma}z_k^{\mathrm{Com}_i(k)}}\\+\dfrac{1}{\gamma}\pi_t^{\mathrm{CDL}}P^{\mathrm{Com}}\mathrm{e}^{-\frac{1}{\gamma}z_k^{\mathrm{Com}}}\left(z_k^{\mathrm{Com}}-z_k^{\mathrm{Com}_i(k)}\right)\\+\sum_{t=1}^{T}\left(\pi_t^{\mathrm{TOU}}P_t^{\mathrm{buy}}+\pi_t^{\mathrm{FIT}}P_t^{\mathrm{sell}}\right)\Delta t\end{array}\right\}\tag{56}$$

Solve the linearized convex optimization problem to obtain $\boldsymbol{\theta}_{k+1}$, $C^{\mathrm{E}}\left(\boldsymbol{\theta}_{k+1}\right)$, $\hat{R}^{\mathrm{CDL}}\left(\boldsymbol{\theta}_{k+1};\boldsymbol{\theta}_k\right)$, $\hat{C}^{\mathrm{Com}}\left(\boldsymbol{\theta}_{k+1};\boldsymbol{\theta}_k\right)$ and compute $R^{\mathrm{CDL}}\left(\boldsymbol{\theta}_{k+1}\right)$, $C^{\mathrm{Com}}\left(\boldsymbol{\theta}_{k+1}\right)$. Use $\left(\boldsymbol{\theta}_{k+1}, R^{\mathrm{CDL}}\left(\boldsymbol{\theta}_{k+1}\right)\right)$ as the next iteration point. When the following formula is satisfied, convergence is considered to be achieved:

$$0\le C^{\mathrm{Com}}(\boldsymbol{\theta}_k)-C^{\mathrm{Com}}\left(\boldsymbol{\theta}_{k+1}\right)\le\varepsilon\tag{57}$$

where ε is the given convergence gap.

To sum up, the entire solving process is shown in Algorithm 1.

Algorithm 1: Concave-convex procedure (CCP) Algorithm

1: **Input**: an initial feasible point $\boldsymbol{\theta}_0$

2: **Repeat** $k=k+1$:

3: The upper bound function is obtained based on (54).

4: Solve the optimization subproblem based on (56).

5: Update $\boldsymbol{\theta}_{k+1}=\left[z^{\mathrm{Com}},P_t^{\mathrm{buy}},P_t^{\mathrm{sell}}\right]^{\mathrm{T}}$ based on (56).

6: Until (57).

7: **Output:** $\boldsymbol{\theta}_{k+1}$.

8: **End**

The basis for Equation (57) lies in the fact that during the optimization of the subproblem $\min\hat{C}^{\mathrm{Com}}\left(\boldsymbol{\theta};\boldsymbol{\theta}_k\right)$, the original objective function value $C^{\mathrm{Com}}(\boldsymbol{\theta})$ is non-increasing [34]. This is a key advantage of the CCP algorithm, ensuring that the original objective function value does not oscillate during iteration and guaranteeing convergence to the optimal value.

The convergence proof of the CCP algorithm is as follows.

In the k-th iteration, let the optimal solution of $\min\hat{C}^{\mathrm{Com}}\left(\boldsymbol{\theta};\boldsymbol{\theta}_{k-1}\right)$ be $\boldsymbol{\theta}_k$.

For the objective function $\hat{C}^{\mathrm{Com}}\left(\boldsymbol{\theta};\boldsymbol{\theta}_k\right)=-\hat{R}^{\mathrm{CDL}}(\boldsymbol{\theta};\boldsymbol{\theta}_k)+C^{\mathrm{E}}(\boldsymbol{\theta})$ in the (k+1)-th iteration, we have:

$$C^{\mathrm{Com}}(\boldsymbol{\theta}_k)=\hat{C}^{\mathrm{Com}}(\boldsymbol{\theta}_k;\boldsymbol{\theta}_k)\tag{58}$$

Also for $\min\hat{C}^{\mathrm{Com}}\left(\boldsymbol{\theta};\boldsymbol{\theta}_k\right)$ in the k+1-th iteration, the optimal solution is $\boldsymbol{\theta}_{k+1}$. This solution satisfies:

$$\hat{C}^{\mathrm{Com}}\left(\boldsymbol{\theta}_{k+1};\boldsymbol{\theta}_k\right)=-\hat{R}^{\mathrm{CDL}}(\boldsymbol{\theta}_{k+1};\boldsymbol{\theta}_k)+C^{\mathrm{E}}(\boldsymbol{\theta}_{k+1})\tag{59}$$

$$C^{\mathrm{Com}}\left(\boldsymbol{\theta}_{k+1}\right)=-R^{\mathrm{CDL}}\left(\boldsymbol{\theta}_{k+1}\right)+C^{\mathrm{E}}(\boldsymbol{\theta}_{k+1})\tag{60}$$

Given the properties of the convex function,

$$R^{\mathrm{CDL}}\left(\boldsymbol{\theta}_{k+1}\right)\ge\hat{R}^{\mathrm{CDL}}\left(\boldsymbol{\theta}_{k+1};\boldsymbol{\theta}_k\right)\tag{61}$$

Thus, the original objective function value $C^{\mathrm{Com}}(\boldsymbol{\theta}_{k+1})$ satisfies:

$$C^{\mathrm{Com}}\left(\boldsymbol{\theta}_{k+1}\right)\le\hat{C}^{\mathrm{Com}}\left(\boldsymbol{\theta}_{k+1};\boldsymbol{\theta}_k\right)\tag{62}$$

Since $\left(\boldsymbol{\theta}_{k+1},\hat{C}^{\mathrm{Com}}\left(\boldsymbol{\theta}_{k+1};\boldsymbol{\theta}_k\right)\right)$ is the optimal point for the objective function $\hat{C}^{\mathrm{Com}}\left(\boldsymbol{\theta};\boldsymbol{\theta}_k\right)$ in the k+1-th iteration, it must satisfy:

$$\hat{C}^{\mathrm{Com}}\left(\boldsymbol{\theta}_{k+1};\boldsymbol{\theta}_k\right)\le\hat{C}^{\mathrm{Com}}\left(\boldsymbol{\theta}_k;\boldsymbol{\theta}_k\right)\tag{63}$$

From equations (58)-(63):

$$C^{\mathrm{Com}}(\boldsymbol{\theta}_k)=\hat{C}^{\mathrm{Com}}(\boldsymbol{\theta}_k;\boldsymbol{\theta}_k)\ge\hat{C}^{\mathrm{Com}}\left(\boldsymbol{\theta}_{k+1};\boldsymbol{\theta}_k\right)\ge C^{\mathrm{Com}}\left(\boldsymbol{\theta}_{k+1}\right)\tag{64}$$

Thus:

$$C^{\mathrm{Com}}(\boldsymbol{\theta}_k)\ge C^{\mathrm{Com}}\left(\boldsymbol{\theta}_{k+1}\right)\tag{65}$$

Hence, the iterative sequence $\left\{C^{\mathrm{Com}}(\boldsymbol{\theta}_k)\right\}_{k=0}^{\infty}$ is a non-increasing convergent sequence.

C. Updated two-step framework with the improvements

In summary, the entire process of the two-step framework is as follows.

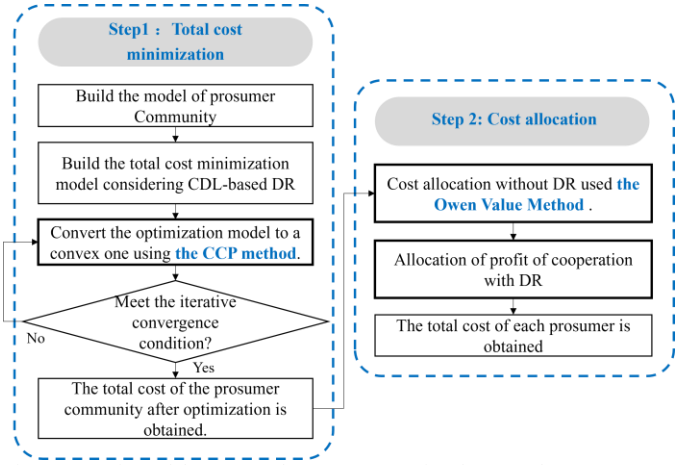

Fig. 3 Overview of the proposed two-step operation framework.

V. Case Study

A. Parameter settings

Taking a prosumer community as an example, this community includes one PV operator, one RU with flexible loads, one parking lot operator with CS and one distributed ES operator. The PV operator and the RU sign a consumption contract, forming a priority coalition. Relevant parameters and values are shown in Appendix A.

Four typical scenarios are studied, as shown in Table I. The detailed results are provided and discussed in the following sub-sections, as shown in Table II.

TABLE I FOUR SCENARIOS STUDIED.

Factors	Scenario			
	1	2	3	4
CDL-based DR	√	×	√	×
Energy sharing transactions in community	√	√	×	×

√/×: Consider the factor or not.

TABLE II THE ANALYSIS DONE WITH THE RELEVANT SCENARIOS.

Analysis	Subsection	Scenario			
		1	2	3	4

CCP iteration	B	√	×	×	×
Benefits of participating in CDL-based DR	C	√	√	√	√
Individual prosumer's power curves	D	√	√	√	√
Prosumers' cost allocation	E	√	√	√	√
Sensitivity of incentive price $\pi^{\mathrm{CDL}}$and deviation coefficient γ	F	√(multiple examples)	×	×	×
Absolute value relaxation results	Appendix B	√(multiple examples)	×	×	×

√: scenario included; ×: scenario not included;
Unless otherwise specified, √ indicates a case constructed with default parameter values.

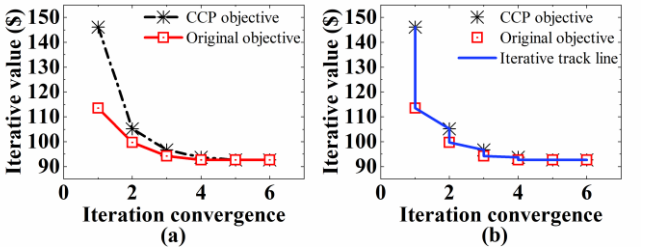

Fig. 4 Optimization objective iteration values based on CCP method in scenario 1: (a) the iteration curves of CCP and original objective, respectively; (b) the combined iteration curve of CCP and original objective.

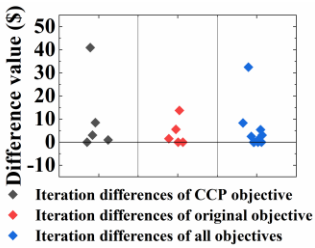

Fig. 5 Distribution of optimization objective iteration differences values based on CCP method in scenario 1

B. *Analysis of CCP iteration results*

This subsection uses Scenario 1 with default values \$0.02/kWh and 0.04 for the incentive price R^{CDL} and deviation coefficient γ.

As outlined in Section IV, the non-increasing convergence of the original objective function is critical when applying the CCP method, as it guarantees convergence to the optimal value. Thus, analyzing the iteration results is necessary to confirm this convergence.

Before analyzing the CCP iteration results, Appendix B examines the validity of the absolute value relaxation method used in Section IV. Linear fitting and visualization demonstrate that the optimization results of the relaxed inequality (47) satisfy the original equation (46).

The following is the analysis of the CCP iteration results.

Fig. 4 shows the iteration results for scenario 1. In both figures, the black dots represent the iterative values of CCP objective $\hat{C}^{\mathrm{Com}}(\boldsymbol{\theta}_k;\boldsymbol{\theta}_{k-1})$, and the red dots represent the iterative values of original objective $C^{\mathrm{Com}}(\boldsymbol{\theta}_k)$.

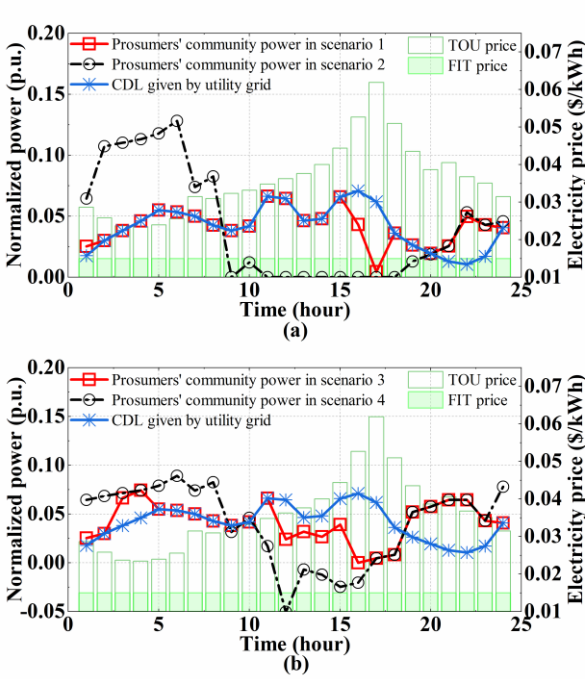

Fig. 6 Results of CDL-based DR: (a) Scenarios 1 and 2; (b) Scenarios 3 and 4.

In Fig. 4(a), both iteration values of $\hat{C}^{\mathrm{Com}}(\boldsymbol{\theta}_k;\boldsymbol{\theta}_{k-1})$ and $C^{\mathrm{Com}}(\boldsymbol{\theta}_k)$ decrease with the number of iterations and meet the convergence criteria by the 5th iteration, respectively. The 6th iteration is included to illustrate that the objective values stabilize, as the values in the 5th and 6th iterations are identical, further confirming the convergence of the CCP algorithm.

In Fig. 4 (b), these value dots are connected in the order $C^{\mathrm{Com}}(\boldsymbol{\theta}_k) \rightarrow \hat{C}^{\mathrm{Com}}(\boldsymbol{\theta}_{k+1};\boldsymbol{\theta}_k) \rightarrow C^{\mathrm{Com}}(\boldsymbol{\theta}_{k+1})$ by a blue solid line. They also decrease with such order as the line shows. This line represents the iterative process associated with equation (64).

The differences in connection styles between Fig. 4 (a) and Fig. 4 (b) are intentional. Fig. 4 (a) focuses on highlighting the independent convergence behavior of the two objective functions, while Fig. 4 (b) provides a clearer visualization of the iterative trajectory as outlined in equation (64). This distinction helps convey different aspects of the CCP iteration process.

The differences between iterations provide a clearer view of CCP algorithm's results. As shown in Fig. 5, the differences between consecutive discrete points along each curve of Fig. 4 are non-negative, indicating that the CCP algorithm's objective functions is decreasing with the number of iterations. This analysis focuses on the differences between each iteration, calculated as the objective value of the current iteration minus that of the next iteration, starting from the 1st iteration. The zero difference between the 5th and 6th iterations demonstrates that the objective value has stabilized, further confirming the convergence of the CCP algorithm.

This analysis aligns with the proof process in equations (62), (64) and (65), demonstrating that the CCP method is effectively applied in this study.

C. Analysis of the prosumer community's CDL-Based DR results

This subsection uses Scenario 1-4 with default values \$0.02/kWh and 0.04 for the incentive price R^{CDL} and deviation coefficient γ.

Fig. 6 shows the normalized power value $P_t^{\mathrm{Com},*}$ of the prosumer community for Scenarios 1 and 2 in (a) and 3 and 4 in (b), both along with the given CDL value $P_t^{\mathrm{CDL},*}$, the given electricity prices π_t^{TOU} and π_t^{FIT}.

In Scenario 1, the normalized power curve of the prosumer community closely follows the CDL curve, deviating only at hours 16, 17, 21, 22, and 23. This indicates strong tracking ability. At hour 17, the overall power of the prosumer community is zero. This is likely due to the high TOU electricity price at that time, leading the prosumer community to avoid purchasing electricity. In Scenario 2, the prosumer community does not participate in CDL-based DR. The normalized power curve follows the price fluctuations. During hours 1-6, when TOU price is low, the prosumer community chooses to purchase electricity. During hours 11-18, when TOU price is high, the overall power of the prosumer community drops to zero.

In Scenario 3, the normalized power curve of the prosumer community overlaps with the CDL curve only during hours 1, 2, and 5-11. At other times, it either lies between the normalized power curve of Scenario 4 and the CDL curve, or coincides with the normalized power curve of Scenario 4. The lower response activity in Scenario 3 is due to the inability of prosumers to share energy. This makes the cost of changing power for CDL-based DR higher than in Scenario 1.

D. Analysis of each prosumer's power curves

This subsection uses Scenario 1-4 with default values \$0.02/kwh and 0.04 for the incentive price R^{CDL} and deviation coefficient γ.

Fig. 7 shows the power each prosumer in Scenarios 1 to 4.

Comparing Scenarios 2 and 4, the prosumer community's power curves are smoother with internal energy sharing. Storage can fully absorb PV generation power and discharge it when needed. This ensures the full utilization of internal energy.

In Scenarios 1 and 2, the positive and negative energy of each prosumer at the same time are considered as internally shared energy. Only the net value is settled externally. This reduces overall costs since the offset energy does not incur external transaction costs. In Scenario 4, without energy sharing, prosumers exhibit different power curves to minimize individual costs. Storage systems may engage in price arbitrage based on varying electricity prices, causing larger fluctuations in power curves.

Comparing Scenarios 1 and 2, with current CDL-based DR incentives, prosumers adjust power values during certain periods to align with the CDL. Despite increasing external energy purchase costs, the incentives provided by the grid cover these additional costs, encouraging prosumers to adjust the overall power curve. This conclusion is also supported by the data analysis presented in Table III. Compared to Scenario 2, the total cost in Scenario 1 decreases from \$145.87 to \$92.72, despite the increase in electricity costs from \$145.87 to \$178.48.

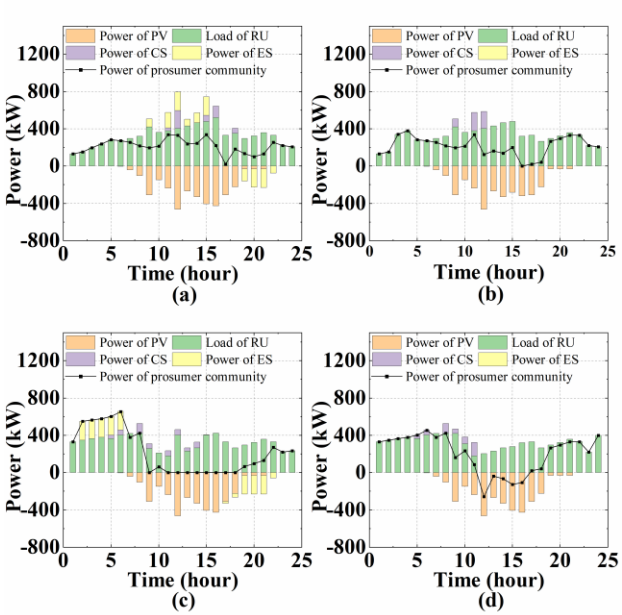

Fig. 7 Bar/line charts of power for each prosumer: (a) Scenario 1; (b) Scenario 2; (c): Scenario 3; (d) Scenario 4.

TABLE III COSTS OF THE PROSUMER COMMUNITY IN DIFFERENT SCENARIOS.

Costs of prosumer community (\$)	Scenarios			
	1	2	3	4
CDL based DR revenue	-85.76	0	-59.73	0
Utility electricity cost	178.48	145.87	253.86	238.26
Total cost	92.72	145.87	194.13	238.26

Positive values indicate costs; negative values indicate revenue or profit.

TABLE IV EACH PROSUMER'S COST.

Prosumer	Costs (non-cooperation) (\$)	Costs (cooperation without DR) (\$)	Net profits (cooperation with DR) (\$)	Costs (cooperation with DR) (\$)
PV	-50.17	-94.53	0	-94.53
RU	273.94	229.57	-24.60	204.97
CS	14.49	13.81	-7.74	6.07
ES	0	-2.98	-20.81	-23.79
Sum	238.26 (scenario 4)	145.87 (scenario 2)	-53.15	92.72 (scenario 1)

Positive values indicate costs; negative values indicate revenue or profit.

E. Analysis of prosumers' cost allocation

This section allocates costs for Scenario 1 using data from Scenarios 1, 2, and 4, with default values \$0.02/kwh and 0.04 for the incentive price R^{CDL} and deviation coefficient γ.

Table III presents the CDL-based DR revenue, utility electricity costs, and total costs for the prosumer community across four scenarios. The total costs for Scenarios 1, 2, and 4 decrease sequentially, indicating that directrix-based demand response and internal sharing transactions help reduce overall costs, especially the latter.

Comparing Scenarios 1 and 2, while Scenario 1 deviates from the optimal purchasing strategy of Scenario 2, increasing electricity costs from \$145.87 to \$178.48, the total cost significantly drops from \$145.87 to \$92.72 due to an \$85.76 DR

revenue. Similarly, the total cost in Scenario 3 decreases from \$238.26 to \$194.13 when compared to Scenario 4. This is consistent with the illustration in Fig. 2.

Overall, participating in CDL-based DR slightly increases the electricity cost of the prosumer community, but the incentive revenue from DR significantly lowers the total cost, motivating the community to adjust the overall power shape.

Additionally, without energy sharing within the prosumer community, a comparison between Scenarios 3 and 1 shows an increase in total electricity purchase cost from \$178.48 to \$253.86, while the CDL-based DR revenue decreases from \$85.76 to \$59.73. The absence of internal energy sharing raises the cost of adjusting unit power in Scenario 3, reducing the community's willingness to align the overall power curve with CDL.

Table IV shows the cost allocation data for each sub-step and the final cost distribution among prosumers in Scenario 1.

Costs (non-cooperation) shows the costs for each prosumer in a non-cooperative state, summing up to the total cost of Scenario 4. Costs (cooperation without DR) corresponds to the first sub-step, with the total cost equating to Scenario 2. The total cost after cooperation is significantly lower due to effective local consumption of PV rather than purchasing from the utility grid. In the first sub-step, the Owen value method is applied. A more detailed explanation of the Owen value method results is provided in Appendix C.

Net profits (cooperation with DR) correspond to the second sub-step, with the net profit for each prosumer being the difference between Scenarios 1 and 2. As shown in Table III, Scenario 1 has CDL-based DR revenue but higher electricity costs, whereas Scenario 2 has lower electricity costs but no DR revenue, resulting in a negative profit difference.

In the second sub-step, the net profit is allocated based on the sum of the absolute value of power changes for each prosumer, referring to the first sub-step. In Appendix C, Fig. C1 illustrates the absolute values of power adjustments, and Fig. C2 presents the adjustment proportion of each prosumer $I_j^{(2)}$ calculated from Equation (41). The analysis below combines insights from Fig. C1, C2, and Table IV. Since PV has no power change, its revenue allocation is zero; RU, CS, and ES have revenue of -\$24.60, -\$7.74, and -\$20.81, respectively, with a total revenue of -\$53.15. RU and ES, with the largest adjustments, bear more net profits, followed by CS, while PV, having no adjustments, receives no allocation. This method ensures fair allocation based on actual contributions.

F. Sensitivity analysis of incentive price and deviation coefficient

This subsection analyzes the impact of DR incentive price π^{CDL} and deviation coefficient γ on the optimization results of the prosumer community in Scenario 1. The utility grid company increases the incentive price from \$0.01/kwh to \$0.08/kwh and the deviation coefficient from 0.01 to 0.08.

Fig. 8 shows the total deviation z^{Com} and the electricity cost C^{E}. Fig. 9 shows the sensitivity analysis of the similarity value S^{Com} and the incentive revenue R^{CDL}. Fig. 10 shows the sensitivity analysis of the total cost of the prosumer community.

In Fig. 8, the black line demarcates the boundary between cases where z^{Com} and C^{E} remain constant despite changes in the deviation coefficient γ and incentive price π^{CDL}, and cases where these variables become sensitive to such changes. Above the solid line, z^{Com} stays at its minimum value of 0.0071, and C^{E} stays at its maximum value of \$178.48, indicating that the optimization results are not influenced by varying γ or π^{CDL} in these regions. The line is drawn to highlight this insensitivity threshold based on these consistent values across the varying parameters.

The minimum value of z^{Com} reflects the limit of the prosumer community 's ability to adjust its power in response to the CDL. At this point, the prosumer community has reached its flexibility limit and cannot further reduce z^{Com} to obtain more incentive revenue.

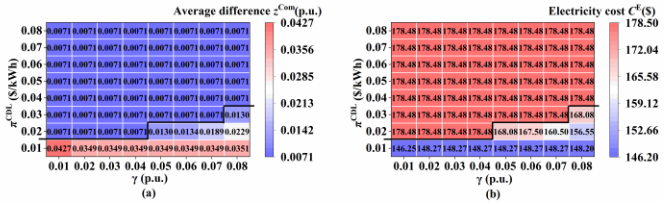

Fig. 8 Sensitivity analysis of (a) weighted average difference and (b) electricity cost (Scenario 1) of the prosumer community.

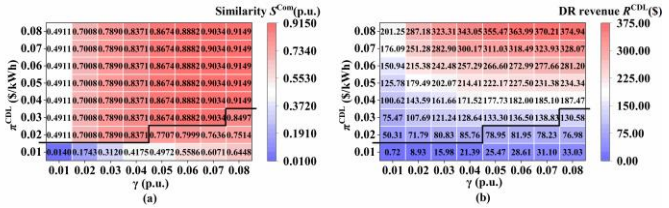

Fig. 9 Sensitivity analysis of (a) similarity value and (b) DR revenue (Scenario 1) of the prosumer community.

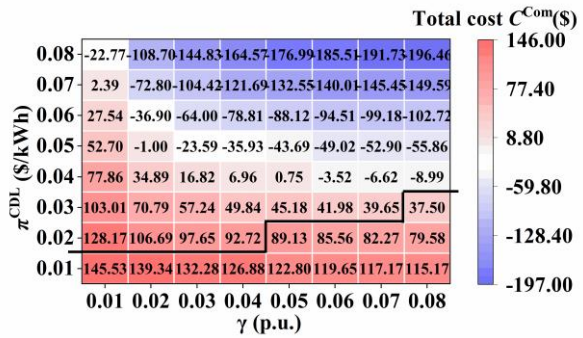

Fig. 10 Sensitivity analysis of total cost (Scenario 1) of the prosumer community.

C^{E} is related to $\left(P_t^{\mathrm{buy}}+P_t^{\mathrm{sell}}\right)$, and $\left(P_t^{\mathrm{buy}}+P_t^{\mathrm{sell}}\right)$ satisfies equality constraints (2), (3) and (13) with z^{Com}. Therefore, when z^{Com} is constant, C^{E} also remains constant. This indicates that in cases above the solid line, the DR revenue covers the cost of power adjustment, so the prosumer community prioritizes adjusting the power curve to participate in DR, even if it increases C^{E}, until the limit of power is reached.

According to equations (4) and (5), there is a quantitative relationship between S^{Com} and z^{Com}, as well as between R^{CDL}

and z^{Com}. Combined with equation (1), a quantitative relationship exists between C^{Com} and z^{Com}, C^{E}. Therefore, the sensitivity characteristics of z^{DL} and C^{E} to two parameters in Fig. 8 is also reflected in S^{DL}, R^{CDL}, and C^{Com}.

Considering the sensitivity characteristics of z^{Com} and C^{E}, black solid lines marking the boundaries, as shown in Fig. 8, have also been added to the corresponding positions in Fig. 9 and Fig. 10 to aid in the sensitivity analysis.

From Fig. 9(a), in cases above the solid line, S^{Com} is sensitive only to the deviation coefficient, not the incentive price. In these cases, z^{Com} remains unchanged, so changes in the incentive price and deviation coefficient do not affect the optimal solution $\boldsymbol{\theta}$ of the model. According to equation (4), when z^{Com} is constant, S^{Com} is related only to the deviation coefficient. Treating z^{Com} as a constant and the deviation coefficient as a variable, the relationship between S^{Com} and the deviation coefficient can be quantitatively analyzed using equation (4).

From Fig. 9(b), in cases above the solid line, R^{CDL} is sensitive to both the incentive price and the deviation coefficient. In these cases, z^{Com} remains unchanged, so changes in the incentive price and deviation coefficient is not significantly affecting the optimal solution $\boldsymbol{\theta}$ of model. According to equations (4) and (3), R^{CDL} is related to both the incentive price and the deviation coefficient. Treating z^{Com} as a constant and the incentive price and deviation coefficient as variables, the relationships between R^{CDL} and these parameters can be quantitatively analyzed using equations (4) and (3).

The above analysis shows that in these cases, the optimal solution $\boldsymbol{\theta}$ is not sensitive to changes in the incentive price and deviation coefficient. As a result, in these cases, even when these two parameters vary, the optimal values of z^{Com} and C^{E} remain constant. S^{Com} and R^{CDL} show clear sensitivity to these parameters and can be analyzed quantitatively.

However, in cases below the solid line, the prosumer community balances the benefits between R^{CDL} and C^{E}. Thus, the optimal solution $\boldsymbol{\theta}$ changes with the incentive price and deviation coefficient significantly. In these cases, the optimal values of z^{Com} and C^{E} depend on the parameter values.

Despite this, Fig. 10 shows the qualitative relationship between the total cost C^{Com} and the parameters. When the deviation coefficient is constant, increasing the incentive price reduces C^{Com}. When the incentive price is constant, increasing the deviation coefficient reduces C^{Com}. Thus, C^{Com} is positively correlated to the deviation coefficient and negatively correlated to the incentive price.

Based on this analysis, setting appropriate parameter values in scenario analysis can effectively encourage prosumers' participation in CDL-based DR while balancing the utility grid company's interest, aligning with realistic application more closely.

VI. Conclusion

This study explores the issues of power optimization and cost allocation in a prosumer community participating in CDL-based DR. The proposed framework first optimizes power usage to balance electricity cost and DR revenue, followed by a detailed cost allocation process. During cost allocation, the Owen value method is applied, accounting for priority coalitions and excluding coalition scenarios that do not exist in practice, as can occur in traditional Shapley value calculation. To manage the non-convex CDL-based DR objective, the framework employs an iterative CCP algorithm, transforming the problem into solvable convex subproblems. Finally, a case study is conducted with a prosumer community comprising four different types of participants, including a PV operator, a RU with flexible loads, a parking lot operator with CS, and a distributed ES operator. Four scenarios are analyzed to assess CDL-based DR framework. Scenario 1 includes both CDL-based DR and energy sharing transactions, Scenario 2 includes only energy sharing, Scenario 3 focuses solely on CDL-based DR, and Scenario 4 excludes both.

The main findings of the study are summarized as follows:

1) The CCP algorithm ensures convergence by iteratively reducing the objective function approximation, achieving convergence within five iterations in this case study. This confirms the algorithm's ability to efficiently handle the non-convex optimization problem, with a final objective value of \$92.72 in Scenario 1.

2) The prosumer community effectively tracks the CDL curve, indicating strong alignment with the target load profile. In Scenario 1, the similarity value S^{Com} is 0.8371, showing the community's ability to respond to price signals and optimize power usage.

3) Within the prosumer community, internal energy sharing smoothens the power curves of individual prosumers, fully utilizing storage capabilities and reducing external transaction costs. Scenarios that incorporated internal sharing exhibited lower overall costs due to effective local consumption and reduced reliance on external electricity purchases, e.g., \$92.72 in Scenario 1 versus \$194.13 in Scenario 3, and \$145.87 in Scenario 2 versus \$238.26 in Scenario 4.

4) The Owen value method considers priority coalitions and excluding non-existent coalitions, leading to more reasonable cost allocations. In Scenario 2, considering the priority coalition between PV and RU, the Owen value method evaluated only 10 combinations, excluding 6 unrealistic combinations where PV or RU independently form coalitions with other prosumers. Compared to the Shapley value method, which considers all 16 combinations, the alliance cost for PV and RU decreased from \$137.58 to \$135.04. This approach resulted in lower costs for PV and RU, reflecting realistic cooperation state within the community.

5) Participation in CDL-based DR slightly increases electricity costs but significantly lowers total costs due to DR incentives, motivating prosumers to adjust power curves. For example, in Scenario 1, electricity costs increase from \$145.87 to \$178.48, but the total cost drops to \$92.72 due to \$85.76 in DR revenue. The incentives provided by the grid cover

additional costs, encouraging active participation and optimization of power usage.

6) The community's optimal response to CDL is sensitive to changes in the deviation coefficient and incentive price, influencing total costs and DR revenue. Scenarios 1-4 demonstrate that setting the incentive price at \$0.02/kWh and the deviation coefficient at 0.04 is effective. Proper setting of these parameters can effectively balance prosumers' participation and the utility grid company's interests.

In our current work, the regional utility grid company's CDL-based DR price for the prosumer community is fixed. This limits the flexibility of the utility grid company's decisions. Future work will explore strategies for setting dynamic incentive prices for the regional utility grid company.

VII. References

[1] K. Pang, C. Wang, N. D. Hatziargyriou, and F. Wen, "Microgrid Formation and Real-Time Scheduling of Active Distribution Networks Considering Source-Load Stochasticity," *IEEE Trans. Power Syst.*, vol. 39, no. 2, pp. 2801–2813, Mar. 2024, doi: 10.1109/TPWRS.2023.3276008.

[2] Y. Zhou, J. Wu, and W. Gan, "P2P energy trading via public power networks: Practical challenges, emerging solutions, and the way forward," *Front. Energy*, vol. 17, no. 2, pp. 189–197, Apr. 2023, doi: 10.1007/s11708-023-0873-9.

[3] J. Wu, Y. Zhou, and W. Gan, "Smart local energy systems towards net zero: practice and implications from the UK," *CSEE J. Power Energy Syst.*, vol. 9, no. 2, pp. 411–419, 2023.

[4] Y. Yao, C. Gao, S. Li, Y. Zhou, D. Wang, and M. Song, "Comparative study on distributed generation trading mechanisms in the UK and China," *Energy Convers. Econ.*, vol. 3, no. 3, pp. 122–141, 2022, doi: 10.1049/enc2.12056.

[5] X. Li, Y. Liu, L. Guo, X. Li, and C. Wang, "Data-driven Based Uncertainty Set Modeling Method for Microgrid Robust Optimization with Correlated Wind Power," *CSEE J. Power Energy Syst.*, vol. 9, no. 2, pp. 420–432, 2023, doi: 10.17775/CSEEJPES.2021.06330.

[6] Y. Xiang, M. Fang, J. Liu, P. Zeng, P. Xue, and G. Wu, "Distributed Dispatch of Multiple Energy Systems Considering Carbon Trading," *CSEE J. Power Energy Syst.*, vol. 9, no. 2, pp. 459–469, 2023, doi: 10.17775/CSEEJPES.2021.09050.

[7] H. Ren, Y. Zhou, F. Wen, and Z. Liu, "Optimal dynamic power allocation for electric vehicles in an extreme fast charging station," *Appl. Energy*, vol. 349, p. 121497, Nov. 2023, doi: 10.1016/j.apenergy.2023.121497.

[8] W. Gan, M. Yan, Y. Zhou, K. Shu, W. Yao, and J. Wen, "Incentivizing energy and carbon rights transactions among network-constrained energy hubs: Cooperative game with externalities," *Renew. Sustain. Energy Rev.*, vol. 203, p. 114771, Oct. 2024, doi: 10.1016/j.rser.2024.114771.

[9] K. Qiu, W. Gan, Y. Zhou, W. Ming, and J. Wu, "Coordinated Operation of Mobile Emergency Generators and Local Flexible Resources for Distribution Network Resilience Enhancement," presented at the Energy Proceedings, 2024. doi: 10.46855/energy-proceedings-11082.

[10] W. N. Silva, L. F. Henrique, A. F. P. da C. Silva, B. H. Dias, and T. A. Soares, "Market models and optimization techniques to support the decision-making on demand response for prosumers," *Electr. Power Syst. Res.*, vol. 210, p. 108059, Sep. 2022, doi: 10.1016/j.epsr.2022.108059.

[11] C. Feng, F. Wen, S. You, Z. Li, F. Shahnia, and M. Shahidehpour, "Coalitional Game-Based Transactive Energy Management in Local Energy Communities," *IEEE Trans. Power Syst.*, vol. 35, no. 3, pp. 1729–1740, May 2020, doi: 10.1109/TPWRS.2019.2957537.

[12] K. Sirviö, S. Motta, K. Rauma, and C. Evens, "Multi-level functional analysis of developing prosumers and energy communities with value creation framework," *Appl. Energy*, vol. 368, p. 123496, Aug. 2024, doi: 10.1016/j.apenergy.2024.123496.

[13] L. Hou *et al.*, "Optimized scheduling of smart community energy systems considering demand response and shared energy storage," *Energy*, vol. 295, p. 131066, May 2024, doi: 10.1016/j.energy.2024.131066.

[14] L. Ni, F. Wen, W. Liu, J. Meng, G. Lin, and S. Dang, "Congestion management with demand response considering uncertainties of distributed generation outputs and market prices," *J. Mod. Power Syst. Clean Energy*, vol. 5, no. 1, pp. 66–78, Jan. 2017, doi: 10.1007/s40565-016-0257-9.

[15] M. Shah, Y. Zhou, J. Wu, and M. Mowbray, "A review of reinforcement learning based approaches for industrial demand response," *Energy Proc.*, vol. 40, 2024, Accessed: Aug. 10, 2024. [Online]. Available: https://orca.cardiff.ac.uk/id/eprint/167943/

[16] W. Liu, Q. Wu, F. Wen, and J. Østergaard, "Day-ahead congestion management in distribution systems through household demand response and distribution congestion prices," *IEEE Trans. Smart Grid*, vol. 5, no. 6, pp. 2739–2747, 2014.

[17] Q. Qdr, "Benefits of demand response in electricity markets and recommendations for achieving them," US Dept. Energy, Washington, DC, USA, Tech. Rep. Accessed: May 05, 2024. [Online]. Available: https://citeseerx.ist.psu.edu/document?repid=rep1&type=pdf&doi=a6a4ea518799c16a26f76597182df1cd0555c78e

[18] A. Heshmati, "Demand, Customer Base-Line and Demand Response in the Electricity Market: A Survey," *J. Econ. Surv.*, vol. 28, no. 5, pp. 862–888, 2014, doi: 10.1111/joes.12033.

[19] S. Fan, Z. Li, L. Yang, and G. He, "Customer directrix load-based large-scale demand response for integrating renewable energy sources," *Electr. Power Syst. Res.*, vol. 181, p. 106175, Apr. 2020, doi: 10.1016/j.epsr.2019.106175.

[20] Y. Meng, S. Fan, Y. Shen, J. Xiao, G. He, and Z. Li, "Transmission and distribution network-constrained large-scale demand response based on locational customer directrix load for accommodating renewable energy," *Appl. Energy*, vol. 350, p. 121681, Nov. 2023, doi: 10.1016/j.apenergy.2023.121681.

[21] J. Li, P. Zhang, J. Zhao, S. Fan, and G. He, "Optimal Control Method of 5G Base Station Virtual Power Plant Based on Customer Directrix Load," *Power Syst. Technol.*, pp. 1–11, 2023, doi: 10.13335/j.1000-3673.pst.2023.1492.

[22] L. Zhu *et al.*, "Online modeling of virtual energy storage for inverter air conditioning clusters in CDL-based demand response," *Energy Rep.*, vol. 9, pp. 2024–2034, Sep. 2023, doi: 10.1016/j.egyr.2023.04.169.

[23] B. Xu, P. Zhang, G. He, and J. Zhao, "Stackelberg game based control method for water heater cluster using customer directrix load," *Proc. CSEE*, vol. 42, no. 21, pp. 7785–7797, 2022, doi: 10.13334/j.0258-8013.pcsee.211678.

[24] B. Xu, J. Zhao, P. Zhang, S. Fan, and G. He, "Accommodating High Level Renewable Energy Based on Customer Directrix Load and Nash Bargaining," *Autom. Electr. Power Syst.*, vol. 47, no. 15, pp. 1–14, 2023.

[25] S. Hong, S. Zhang, and X. Wang, "Bi-Level Optimization Model for Customer Directrix Load-Based Demand Response in Industrial Parks," in *2023 3rd Power System and Green Energy Conference (PSGEC)*, Aug. 2023, pp. 571–575. doi: 10.1109/PSGEC58411.2023.10255880.

[26] H. Moulin, *Fair Division and Collective Welfare*. The MIT Press, 2003. doi: 10.7551/mitpress/2954.001.0001.

[27] J. W. Bialek and P. A. Kattuman, "Proportional sharing assumption in tracing methodology," *IEE Proc. - Gener. Transm. Distrib.*, vol. 151, no. 4, pp. 526–532, Jul. 2004, doi: 10.1049/ip-gtd:20040351.

[28] S. R. Dabbagh and M. K. Sheikh-El-Eslami, "Risk-based profit allocation to DERs integrated with a virtual power plant using cooperative Game theory," *Electr. Power Syst. Res.*, vol. 121, pp. 368–378, Apr. 2015, doi: 10.1016/j.epsr.2014.11.025.

[29] Y. Cheng, H. Gao, R. Wang, Y. Gao, and J. Liu, "Optimal Strategy for Two Stage Customer Directrix Load Based Demand Response and Profit Sharing - Risk Sharing Decision-making Method for Virtual Power Plant," *Power Syst. Technol.*, vol. 48, no. 2, pp. 799–809, 2024, doi: 10.13335/j.1000-3673.pst.2023.1204.

[30] J. Yang, M. Yang, K. Ma, C. Dou, and T. Ma, "Distributed optimization of integrated energy system considering demand response and congestion cost allocation mechanism," *Int. J. Electr. Power Energy Syst.*, vol. 157, p. 109865, Jun. 2024, doi: 10.1016/j.ijepes.2024.109865.

[31] Z. Li, Q. Guo, H. Sun, and J. Wang, "Sufficient Conditions for Exact Relaxation of Complementarity Constraints for Storage-Concerned Economic Dispatch," *IEEE Trans. Power Syst.*, vol. 31, no. 2, pp. 1653–1654, Mar. 2016, doi: 10.1109/TPWRS.2015.2412683.

[32] X. Wang *et al.*, "A Sustainability Improvement Strategy of Interconnected Data Centers Based on Dispatching Potential of Electric

Vehicle Charging Stations," *Sustainability*, vol. 14, no. 11, Art. no. 11, Jan. 2022, doi: 10.3390/su14116814.

[33] X. Yu, Z. Du, Q. Zhang, and Z. Zou, "Proportional Owen value for the coalition structure cooperative game under the incomplete information," *Xitong Gongcheng Lilun Yu ShijianSystem Eng. Theory Pract.*, vol. 39, no. 8, pp. 2105–2115, 2019, doi: 10.12011/1000-6788-2019-0113-11.

[34] T. Lipp and S. Boyd, "Variations and extension of the convex–concave procedure," *Optim. Eng.*, vol. 17, no. 2, pp. 263–287, Jun. 2016, doi: 10.1007/s11081-015-9294-x.

[35] R. A. Toupin and B. Bernstein, "Some properties of the Hessian Matrix of a Strictly Convex Function.," vol. 1962, no. 210, pp. 65–72, Jan. 1962, doi: 10.1515/crll.1962.210.65.

[36] Y. Sun, P. Babu, and D. P. Palomar, "Majorization-Minimization Algorithms in Signal Processing, Communications, and Machine Learning," *IEEE Trans. Signal Process.*, vol. 65, no. 3, pp. 794–816, Feb. 2017, doi: 10.1109/TSP.2016.2601299.

APPENDIX A: PARAMETERS FOR CASE STUDY

1. Basic Parameters

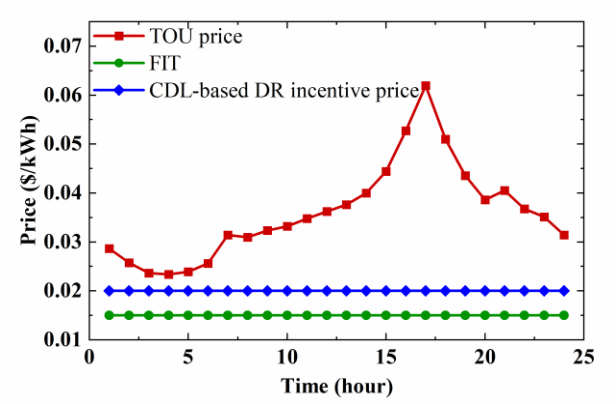

Fig. A1 TOU, FIT and CDL-based DR incentive price.

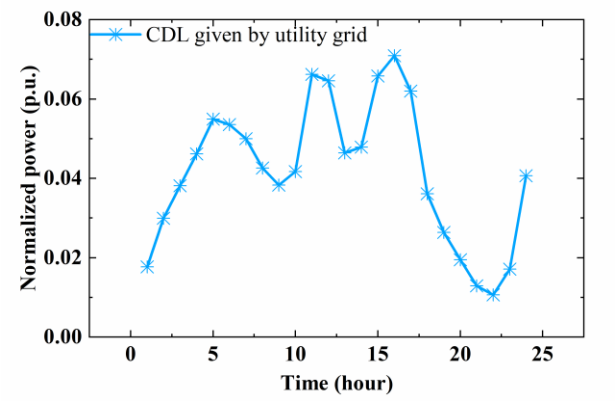

Fig. A2 CDL given by utility grid.

TABLE A1 BASIC PARAMETERS.

Parameter setting	Value	Parameter setting	Value
T	24h	ΔT	1h
γ	0.04		

2. Parameters of RU and PV

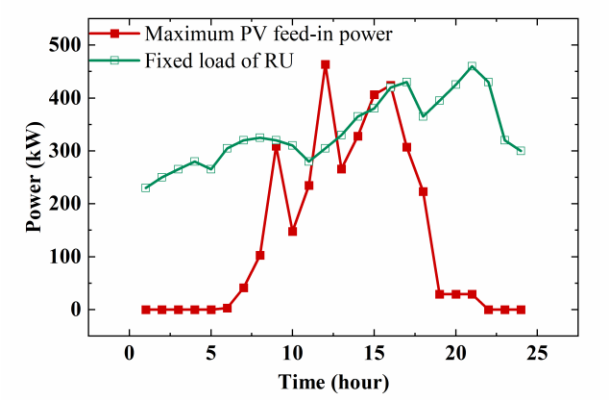

Fig. A3 Fixed Load of RU and maximum PV feed-in Power.

TABLE A2 PARAMETERS OF RU.

Parameter setting	Value	Parameter setting	Value
$P_{j,t,\min}^{\text{Load,move}}$	-100kw	$P_{j,t,\max}^{\text{Load,move}}$	100kw

3. CS Parameters

TABLE A3 PARAMETERS OF CS.

Parameter setting	Value	Parameter setting	Value
N_{EV}	25	$\eta_{\text{EV,ch}}$	0.85
Cap^{EV}	32kwh	$\eta_{\text{EV,dis}}$	0.85
μ_{SOC}	0.5	$P_n^{\text{EV,ch,max}}$	13kW
σ_{SOC}	0.1	$P_n^{\text{EV,dis,max}}$	13kW
μ_{arr}	8.92h	$t_{\text{arr}}^{\min}$	5h
σ_{arr}	3.24h	$t_{\text{arr}}^{\max}$	11h
μ_{dep}	17.47h	$t_{\text{dep}}^{\min}$	15h
σ_{dep}	3.41h	$t_{\text{dep}}^{\max}$	20h
$\text{SOC}_{\min}^{\text{EV}}$	0.3	$\text{SOC}_{\text{exp}}^{\text{EV}}$	1
$\text{SOC}_{\max}^{\text{EV}}$	1		

There are total of N_{EV} EVs in the community. Each EV has a battery capacity of Cap^{EV}, with a charging/discharging efficiency of $\eta_{\text{EV,ch}}$ / $\eta_{\text{EV,dis}}$. The state of charge (SOC) upon arrival, as well as arrival and departure times, follow Gaussian distributions described by equations (A1) - (A3). CS parameter settings are shown in Table A3.

$$S_{\text{SOC}}^{\text{in}} \sim \mathcal{N}(\mu_{\text{SOC}}, \sigma_{\text{SOC}}^2) \quad \text{with} \quad S_{\text{SOC}}^{\min} \le S_{\text{SOC}}^{\text{in}} \le S_{\text{SOC}}^{\max} \tag{A1}$$

$$t^{\text{arr}} \sim \mathcal{N}(\mu_{\text{arr}}, \sigma_{\text{arr}}^2) \quad \text{with} \quad t_{\text{arr}}^{\min} \le t^{\text{arr}} \le t_{\text{arr}}^{\max} \tag{A2}$$

$$t^{\text{dep}} \sim \mathcal{N}(\mu_{\text{dep}}, \sigma_{\text{dep}}^2) \quad \text{with} \quad t_{\text{dep}}^{\min} \le t^{\text{dep}} \le t_{\text{dep}}^{\max} \tag{A3}$$

6. Models of EV

These constraints set the allowable ranges for charging and discharging power and capture the dynamic changes in battery energy.

$$P_{j,t}^{\text{CS,ch}} = \sum_{n=1}^{N} P_{j,n,t}^{\text{EV,ch}} \tag{A4}$$

$$P_{j,t}^{\text{CS,dis}} = \sum_{n=1}^{N} P_{j,n,t}^{\text{EV,dis}} \tag{A5}$$

$$P_{j,t}^{\text{CS,ch}} \le P_{j,t,\max}^{\text{CS,ch}} \tag{A6}$$

$$P_{j,t}^{\text{CS,dis}} \le P_{j,t,\max}^{\text{CS,dis}} \tag{A7}$$

$$0 \le P_{j,n,t}^{\text{EV,ch}} \le \nu_{j,n,t}^{\text{EV}} P_{j,n}^{\text{EV,ch,max}} \tag{A8}$$

$$0 \le P_{j,n,t}^{\text{EV,dis}} \le \nu_{j,n,t}^{\text{EV}} P_{j,n}^{\text{EV,dis,max}} \tag{A9}$$

$$P_{j,n,t}^{\text{EV,ch}} \cdot P_{j,n,t}^{\text{EV,dis}} = 0 \tag{A10}$$

$$E_{\min}^{\text{EV}} \le E_{j,n,t}^{\text{EV}} \le E_{\max}^{\text{EV}} \tag{A11}$$

$$E_{j,n,0}^{\text{EV}} = 0 \tag{A12}$$

$$E_{j,n,t_n^{\text{arr}}}^{\text{EV}} = E_{j,n,\text{arr}}^{\text{EV}} \tag{A13}$$

$$E_{j,n,t_n^{\text{dep}}}^{\text{EV}} = E_{j,n,\text{dep}}^{\text{EV}} \tag{A14}$$

$$E_{j,n,t}^{\text{EV}} = E_{j,n,t-1}^{\text{EV}} + \left(\eta_{\text{EV,ch}} P_{j,n,t}^{\text{EV,ch}} - \frac{1}{\eta_{\text{EV,dis}}} P_{j,n,t}^{\text{EV,dis}} \right) \Delta t \tag{A15}$$

Equations (A4) and (A5) represent total charging and discharging power of all the EVs in the CS. Equations (A6) and (A7) limit CS's maximum charging and discharging power, while (A8) and (A9) ensure each EV's charging and discharging power does not exceed maximum values. Equation (A10) prevents simultaneous charging and discharging. Equation (A11) keeps battery energy within a set range, with (A12) initializing battery energy to zero. Equations (A13) and

(A14) set battery energy at arrival and target departure levels. Finally, equation (A15) describes the temporal evolution of battery energy. These equations form a concise mathematical framework for modeling EV charging and discharging.

Additionally, literature [31] proves that electric vehicles do not simultaneously charge and discharge when their efficiency is not 100%. Since the charging and discharging efficiency in this paper is 0.85, constraint (A10) is therefore omitted.

5. ES Parameters

TABLE A4 PARAMETERS OF ES.

Parameter setting	Value	Parameter setting	Value
$\mathrm{Cap}^{\mathrm{ES}}$	4000kwh	$\eta_{\mathrm{ES,ch}}$	0.85
$\mathrm{SOC}_{\min}^{\mathrm{EV}}$	0.3	$\eta_{\mathrm{ES,dis}}$	0.85
$\mathrm{SOC}_{\max}^{\mathrm{EV}}$	1	$P^{\mathrm{ES,ch,max}}$	500kw
$\mathrm{SOC}_{0}^{\mathrm{ES}}$	0.7	$P^{\mathrm{ES,dis,max}}$	500kw

APPENDIX B: ANALYSIS OF ABSOLUTE VALUE RELAXATION RESULTS

This section is based on Scenario 1 of the Case Study in Section V. The baseline incentive price is increased from \$0.01/kwh to \$0.08/kwh in increments of 0.01, and similarly, the deviation coefficient is varied from 0.01 to 0.08, resulting in 64 cases for comprehensive assessment.

Table B1 shows the effectiveness of relaxing the absolute value equation (46) into inequation (47) in Scenario 1.

The relationship between z_t and x_t is defined as $\begin{cases} z_t = x_t, x_t \geq 0 \\ z_t = -x_t, \ x_t \leq 0 \end{cases}$. For verifying this relationship, we fit the simulation results by a linear function. As shown in Table B1, it is seen that for both $x_t \geq 0$ and $x_t \leq 0$, the intercepts are nearly zero, and the coefficients are exactly 1 and -1, respectively, indicating that the relaxation accurately captures the original equation. The evaluation metrics (MSE, RMSE, and R^2) confirm this conclusion: MSE (Mean Squared Error) measures the average squared difference between predicted and actual values, providing an overall sense of prediction error magnitude. RMSE (Root Mean Squared Error), as the square root of MSE, expresses this error in the same units as the original data, making it more interpretable. R^2 (Coefficient of Determination) measures how well the predicted values align with the actual data. In Table B1, the extremely low MSE and RMSE values suggest minimal error, and the R^2 values of 1.0000 indicate a perfect fit. These results demonstrate that the relaxation approach is highly effective for the absolute value function.

Fig. B1 shows more intuitive fitting results. In the coordinate system $(t_{\mathrm{axis}}, x_{\mathrm{axis}}, z_{\mathrm{axis}})$, a purple plane $\begin{cases} z_{\mathrm{axis}} = |x_t| \\ x_{\mathrm{axis}} = x_t \\ t_{\mathrm{axis}} = t \end{cases}$ is added and the red dots representing (t, x_t, z_t) lie on this plane. The green dots (x, z) are the projections of the red dots onto the x-z plane. By fitting the green dots, it is evident that they lie on the function $z = |x|$ as shown by the dashed green line.

Therefore, the results in Table B1 and Fig. B1 show that the absolute value relaxation constraint satisfies the original absolute value constraint (46). Using the infimum inequality in (47) in place of the original equation yields accurate relaxation results.

TABLE B1 ANALYSIS OF FITTING RESULTS.

Result	$z_t = x_t \ (x_t \geq 0)$	$z_t = -x_t \ (x_t \leq 0)$
Intercept	-2.2078e-09	-8.7640e-18
Coefficient	1.0000	-1.0000
MSE	2.3673e-17	3.7471e-19
RMSE	4.8655e-09	6.1214e-10
R^2	1.0000	1.0000

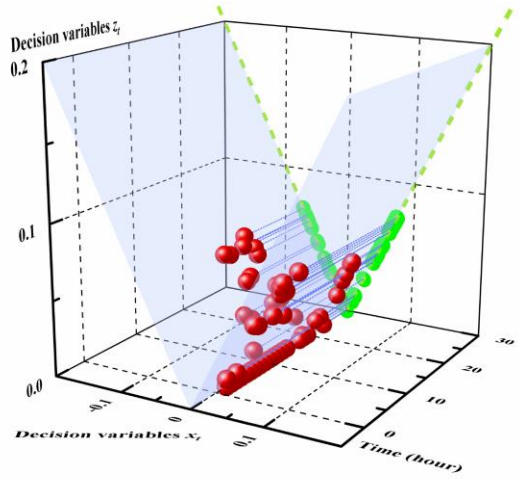

Fig.B1 Visualization of absolute value relaxation results.

APPENDIX C: ADDITIONAL NOTES ON PROSUMERS' COST ALLOCATION ANALYSIS

1. Comparison between Owen and Shapley value methods (with and without priority coalitions)

In the first sub-step of cost allocation, the Owen value method is applied to allocate costs among prosumers within the community. Table C1 compares the results of the Owen and Shapley value methods. When the PV-RU priority coalition is considered, PV's energy is prioritized for RU, resulting in higher costs for CS and ES, while overall costs for PV and RU decrease under the Owen method compared to the Shapley method.

TABLE C1 COST ALLOCATION RESULTS COMPARISON BETWEEN THE OWEN AND SHAPLEY VALUE METHODS IN SCENARIO 2.

Prosumer	Costs (cooperation without DR) (\$)	
	Shapley value method	Owen value method
PV	-91.30	-94.53
RU	228.88	229.57
CS	12.71	13.81
ES	-4.42	-2.98
{PV,RU}	137.58	135.04
Sum	145.87	

Positive values indicate costs; negative values indicate revenue or profit.

Although the results from both methods are similar in

Table C1, the Shapley method considers more coalition combinations, including scenarios unlikely to occur in practice. Thus, the Owen value method offers a more realistic approach.

Table C2 lists all prosumer coalition combinations considered by both the Owen and Shapley value methods, totaling 16, including the empty set. The Shapley value method evaluates costs across all 16 combinations, deriving the cost allocation accordingly. In contrast, the Owen value method accounts for the priority coalition between PV and RU, excluding 6 coalition combinations where PV and RU combine with other prosumers individually, as these are deemed unrealistic.

TABLE C2 COMPARISON OF PROSUMER COALITION COMBINATIONS CONSIDERED BY THE SHAPLEY AND OWEN VALUE METHODS.

Coalition combinations	Shapley value method	Owen value method	Coalition combinations	Shapley value method	Owen value method
{}	√	√	{ES}	√	√
{PV}	√	√	{PV, ES}	√	×
{RU}	√	√	{RU, ES}	√	×
{PV, RU}	√	√	{PV, RU, ES}	√	√
{CS}	√	√	{CS, ES}	√	√
{PV, CS}	√	×	{PV, CS, ES}	√	×
{RU, CS}	√	×	{RU, CS, ES}	√	×
{PV, RU, CS}	√	√	{PV, RU, CS, ES}	√	√

√/×: Consider the coalition combinations or not.

2. Additional notes on the second sub-step of cost allocation

In Appendix C, Fig. C1 illustrates the absolute values of power adjustments over a *T*-hour period for different prosumers, including PV, RU, CS, and ES. The graph highlights that RU and ES have more significant variations in power adjustments compared to PV and CS, indicating their more active roles in responding to CDL.

Fig. C2 presents the adjustment proportion of each prosumer $I_j^{(2)}$ calculated from Equation (41). The chart reveals that RU has the highest adjustment proportion at 0.4628, followed by ES at 0.3916, CS at 0.1456, and PV at 0.0000. This distribution indicates the relative contribution of each prosumer to the overall power adjustment process, with RU and ES playing the most significant roles.

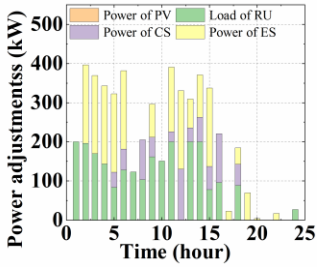

Fig.C1 Absolute values of power adjustments of prosumers.

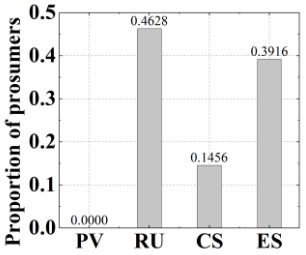

Fig.C2 Proportion of each prosumer's power adjustment to the total adjustments.